



RIGA TECHNICAL  
UNIVERSITY

**Artjoms Supoņenkovs**

# **DEVELOPMENT OF COMPUTER-BASED DIAGNOSTIC SYSTEM IN THE DOMAIN OF MAGNETIC RESONANCE APPLICATIONS**

Summary of the Doctoral Thesis



RTU Press  
Riga 2021

**RIGA TECHNICAL UNIVERSITY**

Faculty of Computer Science and Information Technology

Institute of Smart Computer Technology

**Artjoms Suņņenkovs**

Doctoral Student of the Study Programme “Automation and Computer Engineering”

**DEVELOPMENT OF COMPUTER-BASED  
DIAGNOSTIC SYSTEM IN THE DOMAIN OF  
MAGNETIC RESONANCE APPLICATIONS**

**Summary of the Doctoral Thesis**

Scientific supervisor  
Professor Dr. habil. sc. ing.  
ZIGURDS MARKOVIČS

Scientific consultant  
Assoc. Prof. Dr. med.  
ARDIS PLATKĀJIS

RTU Press  
Riga 2021

Suponenkovs, A. Development of Computer-Based Diagnostic System in the Domain of Magnetic Resonance Applications. Summary of the Doctoral Thesis. Riga: RTU Press, 2021. 53 p.

Published in accordance with the decision of the Promotion Council "RTU P-07" of 4 November 2020, Minutes No. 20-6.

**<https://doi.org/10.7250/9789934225833>**

**ISBN 978-9934-22-582-6 (print)**

**ISBN 978-9934-22-583-3 (pdf)**

# **DOCTORAL THESIS PROPOSED TO RIGA TECHNICAL UNIVERSITY FOR THE PROMOTION TO THE SCIENTIFIC DEGREE OF DOCTOR OF SCIENCE**

To be granted the scientific degree of Doctor of Science (Ph. D.), the present Doctoral Thesis has been submitted for a remote defence at the open meeting of RTU Promotion Council on February 15, 2021 at the following link: <https://rtucloud1.zoom.us/j/97821007392>.

## **OFFICIAL REVIEWERS**

Professor Dr. habil. sc. ing. Jānis Grundspenķis  
Riga Technical University, Latvia

Professor Dr. habil. sc. ing. Irina Arhipova  
Latvia University of Life Sciences and Technologies, Latvia

Professor Dr. habil. sc. ing. Arunas Lukosevicius  
Kaunas University of Technology, Lithuania

## **DECLARATION OF ACADEMIC INTEGRITY**

I hereby declare that the Doctoral Thesis submitted for the review to Riga Technical University for the promotion to the scientific degree of Doctor of Science (Ph. D.) is my own. I confirm that this Doctoral Thesis had not been submitted to any other university for the promotion to a scientific degree.

Artjoms Suponņkovs ..... (signature)

Date: .....

The Doctoral Thesis has been written in Latvian. It consists of Introduction; 5 chapters; Conclusions; 134 figures; 45 tables; 12 appendices; the total number of pages is 219. The Bibliography contains 116 titles.

# CONTENTS

<b>GENERAL DESCRIPTION OF THE DOCTORAL THESIS</b> .....	5
Topicality of the Research.....	5
The Main Aim of the Doctoral Thesis.....	7
Thesis Statements .....	8
The Subject and Object of the Research.....	8
Methods of Research .....	8
Scientific Novelty of the Doctoral Thesis .....	9
Practical Significance of the Doctoral Thesis.....	9
Structure of the Doctoral Thesis.....	12
<b>1. THEORETICAL PART OF THE DOCTORAL THESIS</b> .....	13
1.1. Magnetic Resonance Imaging .....	13
1.2. Knee-Joint and Osteoarthritis.....	14
1.3. MRI Image Processing and Analysis .....	15
<b>2. PROPOSED METHODS AND IMPLEMENTATIONS</b> .....	19
2.1. Calculation of Relaxation Times.....	19
2.2. Visualization of a Knee MRI Scanning Result .....	21
2.3. Tissue Dispersion Analysis .....	23
2.4. Contour Searching in Medical Image .....	24
2.5. Automatic Detection of Increased Synovial Fluid Volume .....	26
2.6. Textual Analysis of Patient’s Information .....	28
2.7. FPGA Optimization .....	30
<b>3. APPROBATION</b> .....	31
3.1. Results of Visualization Methods .....	31
3.2. Results of Histogram Analysis.....	31
3.3. Modulating the Relaxation Process by Many MRI Images .....	32
3.4. Results of Image Pre-Processing and Segmentation.....	33
3.5. Knee-Joint Tissue Recognition .....	34
3.6. Results of Contour Searching in Medical Image .....	37
3.7. Result of Automatic Detection of Increased Synovial Fluid Volume .....	40
<b>RESULTS AND CONCLUSIONS</b> .....	43
<b>APPENDICES</b> .....	45
<b>REFERENCES</b> .....	50

# GENERAL DESCRIPTION OF THE DOCTORAL THESIS

## Topicality of the Research

The knee-joint analysis is very relevant today [1] because of the increasing number of people with knee-joint diseases [2]. The main type of a knee-joint disease is osteoarthritis (OA) [3]. Approximately 27 million Americans have OA. Ramifications of OA are very dangerous: limited range of movement, pain and other problems. Therefore, the analysis of knee-joint soft tissue is very important, especially for OA early diagnostics. The OA early diagnostics allow starting treatment earlier and therefore reducing the risk of knee-joint destruction. The early OA detection offers a chance to completely cure osteoarthritis. It is important for the OA early diagnostics to check the destruction of knee-joint soft tissue. A doctor can check knee-joint soft tissue destruction using the magnetic resonance imaging (MRI) of the knee. MRI is useful for the knee-joint soft tissue presentation [4], but usually a doctor cannot see all necessary information in MRI data [5]. The result of a knee MRI scan contains a lot of information. A radiology technologist, which uses simple (grayscale) images, can see and analyse only a small part of the knee MRI scanning information. This makes it very difficult for a technologist to make an early osteoarthritis diagnosis. Computer MRI analysis makes it possible to process all MRI data and provides additional information for the doctor. This additional information can make it easier to detect invisible injuries of knee-joint soft tissues.

The main source of diagnostic information in this work are medical images. There are several software programs for visualisation and analysis of medical images [6]: MicroDicom, OsirX, OsirX Plugin, ANALYZE, Radiant DICOM<sup>1</sup> Viewer, Slicer, Gimias, and 3D-Doctor. The existing medical image software can be divided into three types:

- 1) simple and convenient software, which are intended mainly for displaying DICOM files and have a convenient interface;
- 2) complex software that has many functions and a complex interface;
- 3) complex software with several modules, which allow expanding the possibilities of the software (usually the modules are intended for the analysis of certain organs).

Unfortunately, the existing universal medical image software have a complex interface and do not have enough image processing tools.

There are several existing tools (programming libraries and modules) that simplify the processing and analysis of medical images [7]: MeVisLab, OpenCV<sup>2</sup>, IDL<sup>3</sup>, MATLAB, ITK<sup>4</sup>. But these tools cannot be used by a doctor. These tools are primarily intended for software developers that can create their own programs using these tools. However, these tools have limitations:

---

<sup>1</sup> DICOM – *Digital Imaging and Communications in Medicine*.

<sup>2</sup> OpenCV – *Open source computer vision*.

<sup>3</sup> IDL – *Interactive Data Language*.

<sup>4</sup> ITK – *Insight Toolkit*.

- 1) the tools contain standard algorithms – often standard algorithms do not have enough capabilities to perform complex tasks (e.g., automatic knee-joint analysis, knee-joint position determination);
- 2) it is usually not possible to improve or change the algorithm of the tool – it means that it is difficult to adapt the algorithm to a specific task;
- 3) integration problems – tool functions and algorithms can work only with certain information formats;
- 4) result representation – the results of tool functions support only specific formats that can be difficult to integrate with other systems;
- 5) some tools are not available for free.

Therefore, the author tries not to use external tools in the development of this work (the external tools are only used for comparison).

Computer OA diagnostics are impossible without segmentation of knee-joint tissues. Before computer OA diagnostics it is important to detect and segment tissue pixels in MRI data. After that, it is possible to do feature analysis of tissue pixels. This distinctive feature analysis allows recognizing different tissue types in the knee-joint. OA damages different types of knee-joint tissue. Therefore, in order to detect injuries of the joint tissues, a comparison of currently analysed tissues with healthy tissues is necessary for computer OA diagnostics. The segmentation of knee-joint tissues allows making a comparison of different tissue pixel groups.

Segmentation of knee-joint tissues by MRI data is a very complicated task, because of the similarity between different soft tissues and MRI data features [8], [9]:

- various image planes (axial, sagittal, coronal);
- many MRI parameters (proton density, relaxation times, magnetic field power) that strongly change the MRI signal;
- different sequences – spin-echo (SE), fast spin-echo (FSE) [10], gradient echo (GRE) and inversion recovery (IR);
- artifacts, patient movement and noise [11].

Therefore, a deep analysis of physical and texture features is necessary for segmentation and recognition of joint tissues.

Obviously, the estimation of patient's knee-joint condition is a quite complex task. This task has many subtasks (Fig 1.):

- 1) estimation, classification and localization of knee-joint tissue;
- 2) analysis of knee-joint tissue by statistical, physical parameters and features;
- 3) analysis of patient disease information;
- 4) acceleration of medical image processing, segmentation and analysis processes;
- 5) displaying of additional information (creation of a visual interface).

In view of the above, there are many unresolved issues that will be addressed in this work.

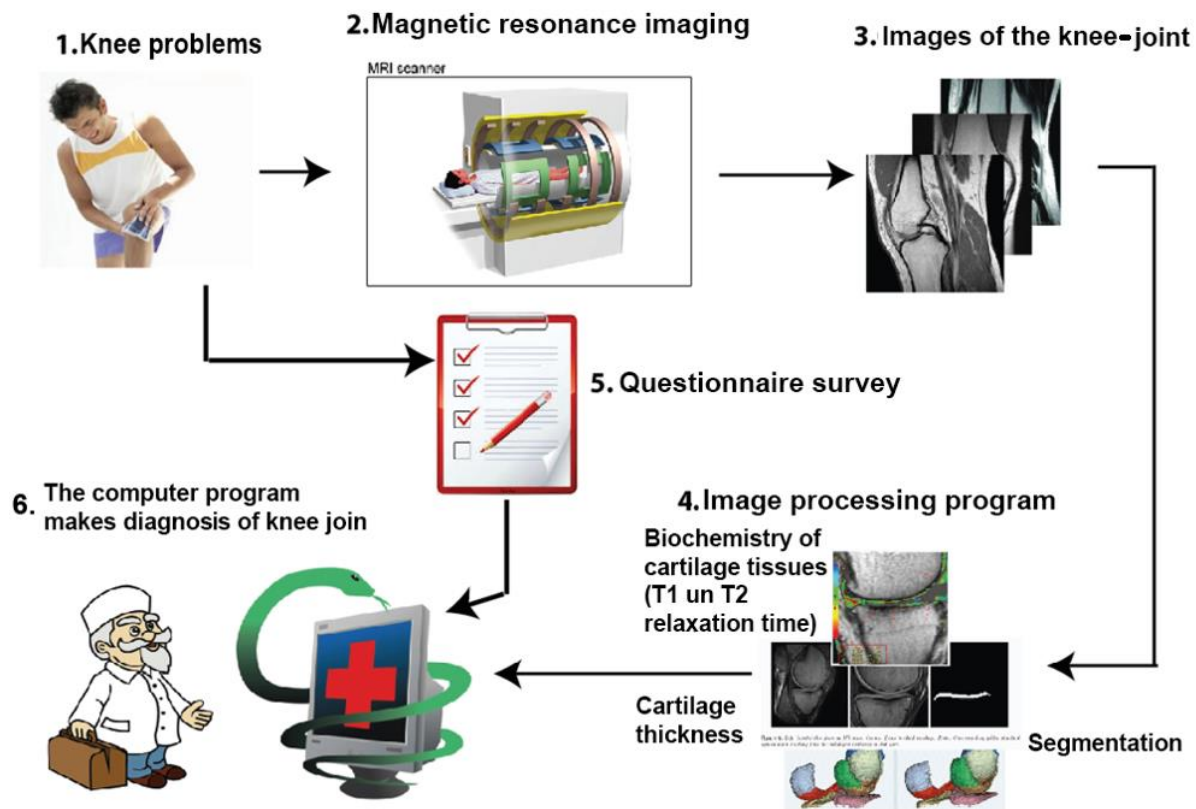


Fig. 1. Common flowchart.

## The Main Aim of the Doctoral Thesis

The aim of the Doctoral Thesis is to develop approaches, methods and algorithms that allow creating digital medical diagnostic systems that could be used for the knee-joint analysis.

In order to achieve the aim of the Doctoral Thesis, it is necessary to solve the following **tasks of the Doctoral Thesis**:

- 1) to develop methods of relaxation time calculation;
- 2) to develop a pre-processing method of medical images that are used to remove artifacts and noise;
- 3) to develop interactive and automatic segmentation methods of medical images that are used to perform segmentation of human body tissue and fluid;
- 4) to develop methods for creation and recognition of human body tissue pattern;
- 5) to develop methods for the analysis of human body tissues and fluids;
- 6) to develop methods, algorithms and implementations for the visualization of human body tissues and fluids;
- 7) to develop methods and computer implementation for calculation of the osteoarthritis severity index and probability index of knee-joint;
- 8) to develop methods of speeding up execution time for image processing and analysis.

As a result of the Doctoral Thesis, six new modules have been developed and are described in the practical part. These new modules have a lot of possibilities: calculation of

relaxation times; segmentation of fluids and tissues of human body, calculation of features and defect detection; pre-processing and visualization of medical image; optimization of medical image processing instruction; textual analysis of patient's information.

### **Thesis Statements**

1. The tissue segmentation and texture feature analysis methods, developed in the author's work, make it possible to distinguish healthy patients from patients with osteoarthritis.
2. The author's proposed medical template matching method allows making automatic detection and localization of fluids and tissues.
3. The author's proposed adaptive watershed method is used to perform automatic detection of synovial fluid augmentation.
4. Statistical features of medical image texture could be helpful for classifying tissues and fluids of human body.

### **The Subject and Object of the Research**

**The subject of the research** is methods and algorithms that are used to process the patient's diagnostic information. These methods and algorithms are medical image pre-processing, methods and algorithms of segmentation and analysis that are used for the analysis of the patient's textual diagnostic information.

**The object of research** is diagnostic information of the patient's knee-joint. This knee-joint diagnostic information contains medical MRI images in DICOM format. Also, this diagnostic information includes a textual description of the patient's medical condition that has been obtained by using DICOM file tags and author's questionnaire.

### **Methods of Research**

The following methods have been used in the Doctoral Thesis:

- 1) classification and observation methods – segmentation of medical image;
- 2) methods of comparison and measurement – statistical analysis of tissues and fluids of human body;
- 3) observation method – visual analysis of enhanced medical images;
- 4) methods of comparison and measurement – analysis of textual description of the patient's medical condition;
- 5) methods of comparison, measurement and induction – analysis of texture and geometric features of tissues and fluids of human body;
- 6) observation method – analysis of medical image noise and artifacts;
- 7) experimental method – template matching;
- 8) modelling method – modelling of  $T_2 / T_1$  relaxation process; and others.

## Scientific Novelty of the Doctoral Thesis

The new achievements are as follows:

- 1) development of automatic methods for fluid and tissue localization and analysis [12, 5], [13, 5], [14, 4];
- 2) development of automatic methods for osteoarthritis diagnosis by using statistical analysis [13, 7], [15], [16, 6];
- 3) development of methods that allow finding unique texture features of medical images of tissues and fluids of human body [17, 5], [18, 5], [14, 3, 5, 6];
- 4) development of MRI image visualisation methods that are used to perform early osteoarthritis diagnostics [13, 4, 6], [16, 5];
- 5) development of methods for speeding up execution time of image processing and analysis. The author's proposed module allows to reduce the runtime of FPGA<sup>5</sup> instruction. Also, it allows to minimize the size of FPGA instruction [19, 4], [20, 8], [21, 6], [22, 7], [23];
- 6) development of module of relaxation time calculation that allows to calculate relaxation time by one, two, or many MRI images [16, 4], [12, 3, 4].

## Practical Significance of the Doctoral Thesis

The practical significance of the Doctoral Thesis is the six new modules. These new modules have a lot of possibilities: calculation of relaxation time; segmentation of fluids and tissues of human body, calculation of features and defect detection; medical image pre-processing and visualization; optimization of medical image processing instruction; textual analysis of patient's information. The results of the Doctoral Thesis have been presented in 11 scientific conferences and published in 10 international scientific papers.

### Publications

1. Suponenkovs A., Markovics Z., Platkajis A. "Knee-joint tissue recognition in magnetic resonance imaging", (2018) IEEE 30<sup>th</sup> Jubilee Neumann Colloquium, NC 2017, 2018-January. (**SCOPUS**) (*Author's contribution – 86 %, writing for publication, software development*).
2. Suponenkovs A., Glazs A., Platkajis A. "Development of methods for analysis of knee articular cartilage degeneration by magnetic resonance imaging data", Journal of Physics: Conference Series, 818 (1), art. No. 012001. Indonesia; (2017) (**SCOPUS**) (*Author's contribution – 86 %, writing for publication, software development*).
3. Suponenkovs A., Markovics Z., Platkajis A. "Computer Analysis of Knee by Magnetic Resonance Imaging Data" (2016) Procedia Computer Science, 104, pp. 354–361. (**SCOPUS**) (*Author's contribution – 86 %, writing for publication, software development*).

---

<sup>5</sup> FPGA – Field-programmable gate array.

4. Suponenkovs A., Grabis, J., Kampars, J., Sisojevs, A., Pinka, K., Mosans, G., Taranovs, R., Locmelis, A. Application of Image Recognition and Machine Learning Technologies for Payment Data Processing Review and Challenges. *2017 5<sup>th</sup> IEEE Workshop on Advances in Information, Electronic and Electrical Engineering (AIEEE 2017) (SCOPUS) (Author's contribution – 80 %, writing for publication, software development)*.
5. Lemberski I., Suponenkovs A. “Asynchronous Logic Design Targeting LUTs”, Budva; Montenegro; 10 June 2018. **(SCOPUS)** *(Author's contribution – 50 %, assistance in writing for publication, software development)*.
6. Lemberski I., Suponenkovs A. “Asynchronous logic one-level LUT design based on partial acknowledgement”, *Microelectronics Journal*, 2018. **(SCOPUS)** *(Author's contribution – 50 %, assistance in writing for publication, software development)*.
7. Suponenkovs A., Kovalovs A., Markovics Z. “Application of Computer Vision Technologies for Autonomous Pile Manipulation”, 12<sup>th</sup> International Scientific and Practical Conference on Environment. Technology. Resources. Rezekne, Latvia, 20 June 2019. **(SCOPUS)** *(Author's contribution – 84 %, writing for publication, software development)*.
8. Lemberski I., Suponenkovs A., Uhanova M. “LUT-Oriented Asynchronous Logic Design Based on Resubstitution”, *Proceedings – 2019 14<sup>th</sup> IEEE International Conference on Design and Technology of Integrated Systems in Nanoscale Era, DTIS 2019, Mykonos, 2019. (SCOPUS) (Author's contribution – 33 %, assistance in writing for publication, software development)*.
9. Suponenkovs A., Platkajis A., Markovics Z. “Application of Magnetic Resonance Imaging and Computer Vision Technologies for Analysis of Knee Articular Cartilage Degeneration.” *Lietuva Radiology Update*, 2018. **(Copernicus)** *(Author's contribution – 86 %, writing for publication, software development)*.
10. Lemberski I., Uhanova M., Suponenkovs A. “Distributed Indication in LUT-Based Asynchronous Logic”, *PdeS 2019, High Tatras, Slovakia. (SCOPUS) (Author's contribution – 33 %, assistance in writing for publication, software development)*.

#### **Publications (submitted for publishing)**

11. Supe I., Suponenkovs A., Platkajis A., Kadisa A., Lejniaks A. “Detecting knee cartilage structural changes using magnetic resonance computed vision analysis in patients with osteoarthritis; preliminary results”, *PROCEEDINGS OF LATVIAN ACADEMY OF SCIENCE*, 2020 **(will be available in SCOPUS)** *(Author's contribution – 40 %, assistance in writing the publication, program development)*.

#### **Research results presented in conferences**

1. 14<sup>th</sup> IEEE International Conference on Design and Technology of Integrated Systems in Nanoscale Era, DTIS 2019, Mykonos, Greece, 2019. (Title of the report – “LUT-oriented asynchronous logic design based on resubstitution”).

2. 7<sup>th</sup> Mediterranean Conference on Embedded Computing, MECO 2018, Budva, Montenegro, 2018. (Title of the report – “Asynchronous logic design targeting LUTs”).
3. 30<sup>th</sup> IEEE Jubilee Neumann Colloquium, NC 2017. Obuda University, Budapest, Hungary, 2017. (Title of the report – “Knee-joint tissue recognition in magnetic resonance imaging”).
4. Congress on Industrial and Applied Life Sciences and Mathematics, Nature-Math. Indonesia. 2016. (Title of the report – “Development of methods for analysis of knee articular cartilage degeneration by magnetic resonance imaging data”).
5. 12<sup>th</sup> International Scientific and Practical Conference on Environment. Technology. Resources. Rezekne, Latvia, 2019. (Title of the report – “Application of Computer Vision Technologies for Autonomous Pile Manipulation”).
6. 5<sup>th</sup> IEEE Workshop on Advances in Information, Electronic and Electrical Engineering, AIEEE 2017, Riga, Latvia. (Title of the report – “Application of image recognition and machine learning technologies for payment data processing review and challenges”).
7. 16<sup>th</sup> IFAC Conference on Programmable Devices and Embedded Systems (PdeS 2019), 2019, High Tatras, Slovakia. (Title of the report – “Distributed Indication in LUT-Based Asynchronous Logic”).
8. 7<sup>th</sup> Baltic Congress of Radiology (BCR) 2018, Kaunas, Lithuania. (Title of the report – “Application of Magnetic Resonance Imaging and Computer Vision Technologies for Analysis of Knee Articular Cartilage Degeneration”).
9. Riga Technical University 59<sup>th</sup> International Scientific Conference. (Titles of reports: “Diagnosis of osteoarthritis by magnetic resonance imaging data and topological model”; “Visualization and preprocessing of MRI scanning result”).
10. Riga Technical University 60<sup>th</sup> International Scientific Conference. (Titles of reports: “Segmentation and Analysis of Knee Joint Tissue”; “Industrial Computer Vision”; “Analysis of Magnetic Resonance and Spectroscopic Material”).
11. Riga Technical University 57<sup>th</sup> International Scientific Conference. (Titles of reports: “Tissue segmentation and analysis by magnetic resonance imaging data”; “DICOM series joining and analyzing”; “DICOM series image processing”).

### **Awards**

Certification of Best Paper Award, Congress on Industrial and Applied Life Sciences and Mathematics, Nature-Math. Indonesia, 2016.

### **Comparison of international results (Best LUT-6 Implementations – 2020)**

[https://github.com/lsils/benchmarks/tree/master/best\\_results](https://github.com/lsils/benchmarks/tree/master/best_results)

## Structure of the Doctoral Thesis

The Doctoral Thesis consists of Introduction, 5 chapters, Conclusions, references and 12 appendices.

**Introduction** gives a general description of the Doctoral Thesis. It contains topicality of the research, the main aim and tasks of the Doctoral Thesis. It also describes scientific novelty, practical significance and results of the work.

**Chapter 1 – Magnetic resonance imaging** – describes physical aspects of the dissertation with the aim to study the dependencies between the physical processes of atoms and the intensities of the pixels (voxels) of the MRI image. It describes the process of the MRI image acquisition and DICOM file format.

**Chapter 2 – Knee-joint and osteoarthritis** – describes medical aspects of the dissertation with the aim to investigate the dependencies between the MRI data and knee-joint conditions. It describes the risk factors and pathogenesis of knee-joint osteoarthritis.

**Chapter 3 – MRI image processing and analysis** – describes mathematical aspects of the dissertation with the aim to study pre-processing, segmentation and analysis methods of medical images. Approaches of pattern search, geometric and texture feature analysis have been analysed in this chapter. It describes the FPGA technology-based accelerating approach for medical image processing and analysis.

**Chapter 4 – Proposed methods and implementations** – describes six new modules developed by the author. These new modules have a lot of possibilities: calculation of relaxation times; segmentation of fluids and tissues of human body, calculation of features and defect detection; medical image pre-processing and visualization; optimization of medical image processing instruction; textual analysis of patient's information.

**Chapter 5 – Approbation of the proposed methods** – shows the experimental results that have been achieved by author's methods. The chapter describes an experiment of image pre-processing, segmentation, and texture analysis. It describes many important experiments: experiment of pattern search, experiment of automatic detection and localization of synovial fluid, experiment of relaxation time calculation, experiment of analysis and visualization of cartilage.

The last chapter – **Main results and conclusions** – shows the main results of the dissertation.

# 1. THEORETICAL PART OF THE DOCTORAL THESIS

## 1.1. Magnetic Resonance Imaging

This chapter describes physical aspects of the dissertation with the aim to study the dependencies between the physical processes of atoms and the intensities of pixels (voxels) of the MRI image. It describes the process of MRI image acquisition and the DICOM file format [24].

Protons of hydrogen atoms are very important in MRI process. The MRI process cycle has 3 stages: 1) initial state – protons of hydrogen atoms are in a strong magnetic field; 2) RF pulse – protons of hydrogen atoms receive energy and move from a low energy level to a high energy level; 3) relaxation process – protons of hydrogen atoms return the energy and go back to their start state. This relaxation process takes some time (relaxation time). There are two relaxation process types: spin-lattice relaxation (takes time  $T_1$ ) and spin-spin relaxation (takes time  $T_2$ ). Spin-lattice relaxation process is the relaxation process of the  $M_z$  component. The spin-spin relaxation process is the relaxation process of the  $M_{xy}$  component. The spin-spin relaxation process may take less time,  $T_2^*$ , because of inhomogeneity of magnetic field.

The value of simple MRI image pixels is dependent on MRI signal ( $S$ ). But the MRI signal is dependent on relaxation times  $T_2$  and  $T_1$  as well as proton density  $\rho$  [9]. We can change the relaxation time and proton density influence on MRI signal. The dependence between the signals and relaxation time for SE (spin-echo signal sequence) is shown in the following Equation (1.1) [9]:

$$S = M_0 \left[ 1 - \exp\left(\frac{-T_R}{T_1}\right) \right] \left[ \exp\left(\frac{-T_E}{T_2}\right) \right], \quad (1.1)$$

where  $M_0$  – initial magnetization or start state,  $T_R$  – time to repeat,  $T_E$  – echo time,  $T_1$  and  $T_2$  – relaxation time, and  $S$  – MRI signal.

The initial magnetization ( $M_0$ ) is foremost depending on proton density and magnetic field power ( $B_0$ ) measured in tesla (T). This is shown in Equation (1.2). Usually is using MRI with 1.0 T, 1.5 T and 3.0 T.

$$M_0 \sim \rho B_0, \quad (1.2)$$

where  $\rho$  – proton density and  $B_0$  – magnetic field power.

By manipulating with  $T_R$  and  $T_E$  parameters we can change the relaxation times and proton density influence on MRI signal. As a result of manipulation with these parameters we can get three types of MRI images:  $T_1$  weighted,  $T_2$  weighted, and proton density (PD) image (Table 1.1) [8]. According to the MRI image type PD/ $T_1$ / $T_2$  the MRI signal foremost is depending on proton density, relaxation time ( $T_1$ ) and relaxation time ( $T_2$ ) [25].

Table 1.1

 $T_R$  and  $T_E$  Parameters for SE Sequence

Sequence	MRI image type	Parameter $T_R$	Parameter $T_E$
SE	$T_1$	600 ms	10–30 ms
	PD	1000 ms	10–30 ms
	$T_2$	2000 ms	80–250 ms

The findings of this chapter are as follows.

1. Soft tissues consist mainly of hydrogen atoms. Therefore, it is useful to analyse hydrogen atoms by MRI. Also, hydrogen atoms have a high value of gyromagnetic ratio that allows getting high-contrast medical images of soft tissues.
2. MRI medical images do not have standard tissue-intense scale (like a Hounsfield scale in CT scans). This means that the same tissue may have different intensity in MRI images with different  $T_R$  and  $T_E$  parameters.
3. The value of MRI image pixels is dependent on proton density, magnetic field power, time to repeat ( $T_R$ ), echo time ( $T_E$ ), and relaxation times  $T_1$  and  $T_2$ .
4. Magnetic resonance imaging (MRI) is the most effective non-invasive technique for analysing and displaying the soft tissue damage. Thus, this work describes new methods for soft tissue diagnostics by magnetic resonance imaging data.

## 1.2. Knee-Joint and Osteoarthritis

An early osteoarthritis diagnosis is very important because it provides a possibility to completely cure osteoarthritis. Chondrocytes make it possible to regenerate cartilage. The knee articular cartilage changes are recoverable at the early stage of OA [26].

Osteoarthritis has 5 grades (Fig 1.1) [27], [28]. Doctors are unable to see the first grade of the OA using simple grayscale MRI images. But the knee articular cartilage changes are recoverable at the first grade of OA. Therefore, displaying of the OA first grade is a very important problem.

Early diagnosis of OA is very important, since it is necessary to start OA treatment as soon as possible. However, it is hard to detect the first grade (cartilage softening) by MRI. Therefore, it is useful to find additional symptoms of the first grade. It is possible to use additional information about biochemical tissue features. The first grade has the following additional MRI symptoms [29]:

- 1) increased proton density (where proton density is the number of hydrogen resonating protons per unit of volume);
- 2) increased  $T_{1\rho}$  relaxation time (where relaxation time is the recovery time of the proton spin magnetization after RF exposure);
- 3) increased  $T_2$  relaxation time.

These symptoms make it possible to detect the first grade of OA.

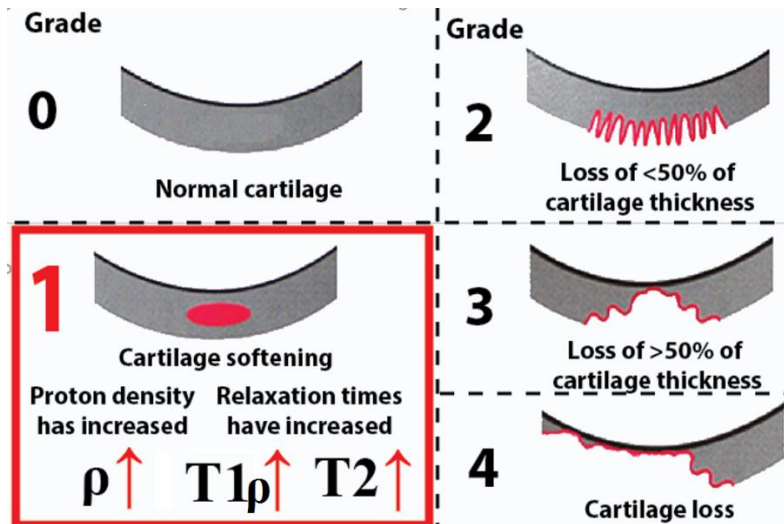


Fig. 1.1. Outerbridge classification [30].

The findings of this chapter are as follows.

1. Chondrocytes make it possible to regenerate cartilage. Therefore, early diagnosis of osteoarthritis (before degeneration of chondrocytes) makes it possible to cure osteoarthritis.
2. It is hard to detect the first grade of OA (cartilage softening) by simple grayscale MRI images. Therefore, it is important to use additional software for OA detection.
3. The first grade of OA has the following features: increase in proton density and in relaxation times. These features make it possible to detect the first grade of OA.
4. There are many MRI signs of OA [31]: gradual wear to the cartilage surface, synovial hypertrophy, joint space narrowing and osteophyte formation [32].

### 1.3. MRI Image Processing and Analysis

This chapter describes mathematical aspects of the dissertation with the aim to study the pre-processing [33], segmentation and analysis methods of medical images. Approaches for the analysis of pattern search, geometric [34], [35] and texture features is presented in this chapter. The chapter also describes the FPGA technology-based accelerating approach for medical image processing and analysis. Special attention is paid to the edge detection algorithms (Fig. 1.2).

The image segmentation makes it possible to perform an analysis of knee. However, segmentation is a very complicated task because MRI image contains a lot of information. Therefore, it is important to remove unnecessary information from MRI image. For this purpose, it is possible to use image preprocessing.

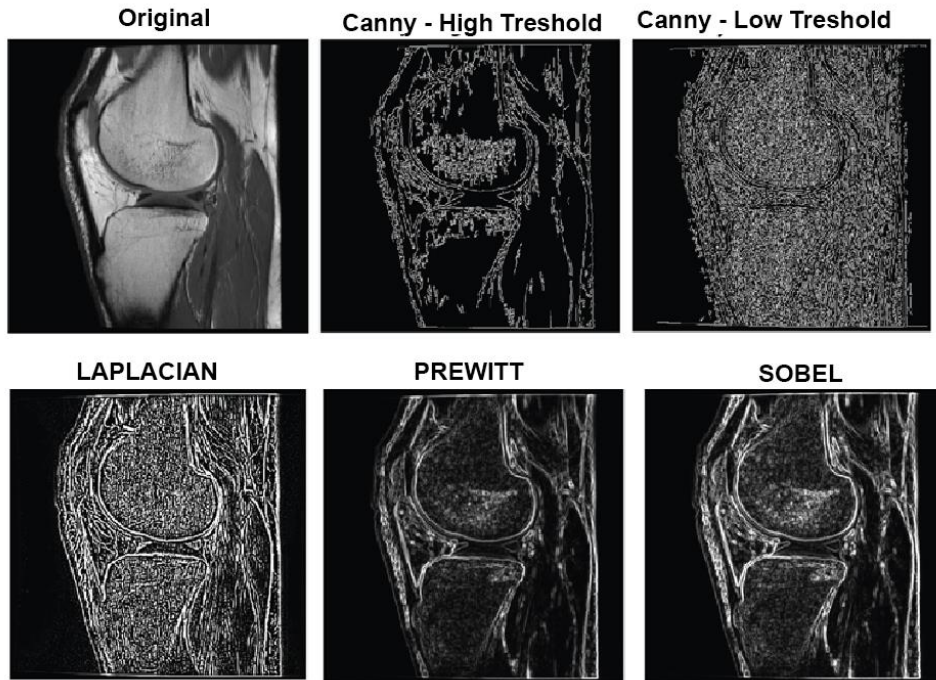


Fig. 1.2. Edge detection algorithms.

Perona–Malik filter is an anisotropic diffusion [36], [37] that removes high frequency components (noise, small details). This filter has an advantage – it does not remove borders of large segments. Therefore, Perona–Malik filter prepares the MRI image for further segmentation. The anisotropic diffusion is described with Equation (1.3):

$$I_t(x, y, t) = \text{div}(c(x, y, t)\nabla I(x, y, t)), \quad (1.3)$$

where  $c$  – special diffusion coefficient;  $I$  – smoothing image (the level of smoothing of the image depends on the  $t$  parameter);  $\text{div}$  – divergence;  $\nabla$  – gradient;  $I_t$  – resulting image.

As shown in Fig. 1.3, the combination of two methods (Perona–Malik filter and  $k$ -means clustering [38]) provided good segmentation results.

The second segmentation type is a watershed segmentation [39]. As shown in Fig. 1.3, this segmentation works well together with Sobel operator. However, the result of watershed segmentation contains a lot of tiny segments. This problem can be solved by using additional information about the knee.

Sometimes, it is necessary to improve the accuracy of segmentation. For this reason, the knee tissue segmentation results could be improved by textural tissue feature analysis. Textural tissue feature analysis can be performed by using a co-occurrence matrix [40].

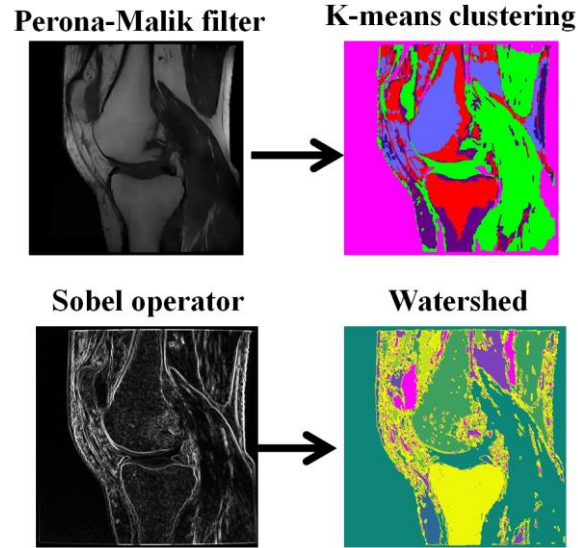


Fig. 1.3. Two types of MRI image segmentation.

Grayscale MRI images have different texture features:

- 1) texture features based on spatial frequencies;
- 2) texture features based on statistical characteristics (GLCM – grey-level co-occurrence matrix [41], [42], histogram);
- 3) texture features based on structural elements (GLRLM – grey-level run length matrix [43], [44], GLSZM – grey-level size zone matrix [45], [46]).

For the calculation of texture features it is advised to use a special matrix or a histogram. In this work, special attention is paid to the GLCM (grey-level co-occurrence matrix). Depending on the matrix direction, there can be four types of this matrix: vertical, horizontal, diagonal (45 degrees) and diagonal (135 degrees). GLCM matrix preparation for the calculation of texture features has 4 steps.

1. Quantization of grey image pixel values – all values of the new image pixels must be in the range (from 0 to GLCM matrix size).
2. GLCM matrix calculation – GLCM matrix shows the frequency of combination of neighbouring elements.
3. GLCM matrix symmetrisation.
4. GLCM matrix normalisation – matrix values must be in the range from 0 to 1.

After that, it is possible to calculate some features of the texture (1.4)–(1.6):

contrast (*CON*):

$$CON = \sum_{i,j=0}^{N-1} P_{i,j} (i - j)^2, \quad (1.4)$$

homogeneity (*HOM*):

$$HOM = \sum_{i,j=0}^{N-1} \frac{P_{i,j}}{1 + (i - j)^2}, \quad (1.5)$$

entropy (*ENT*):

$$ENT = \sum_{i,j=0}^{N-1} P_{i,j} (-\ln P_{i,j}), \quad (1.6)$$

where  $P$  – GLCM matrix value (after normalisation) that shows the probability of combined neighbouring elements;  $i$  and  $j$  – GLCM matrix indexes, which show the quantized image pixels values of neighbouring elements;  $N$  – GLCM matrix size.

It is possible to analyse the segment shape by its geometric features. The circularity can be calculated as follows (1.7):

$$C = \frac{P^2}{S}, \quad (1.7)$$

where  $P$  – segment perimeter, and  $S$  – segment area.

The other important geometric feature is elongation (1.8):

$$Elong = \frac{m_{20} + m_{02} + \sqrt{(m_{20} - m_{02})^2 + 4m_{11}^2}}{m_{20} + m_{02} - \sqrt{(m_{20} - m_{02})^2 + 4m_{11}^2}}, \quad (1.8)$$

where  $m_{20}$  – two-dimensional central moment (2 and 0 is moment index), and  $m_{jk}$  – central moment ( $j$  and  $k$  is moment index).

Sometimes, it is necessary to detect a tissue edge [47]–[50]. There are a lot of edge detection algorithms (Fig. 1.2). The active contour model can be useful for improvement of tissue edge detection [51], [52]. The active contour model can improve the edge detection results by using the energy functional. The energy functional is described with Equation (1.9):

$$E(v) = E_{\text{int}}[v(s)] + E_{\text{ext}}[v(s)], \quad (1.9)$$

where  $E_{\text{int}}$  – internal energy of active contour, and  $E_{\text{ext}}$  – external energy of active contour.

The findings of this chapter are as follows.

1. Perona–Malik filter is an anisotropic diffusion that removes high frequency components (noise, small details). This filter has an advantage – it does not remove the borders of large segments. The disadvantage of this method is the relatively low execution speed.
2. Filters and methods based on the first derivative can be useful for detection of long jumps (oblique jumps) in brightness. But, on the other hand, filters and methods that are based on the second derivative can be useful for detection of short jumps (pulse jumps) in brightness.
3. The active contour model can improve contour searching results by using energy functional.
4.  $k$ -means clustering [53]–[56] result is depending on the number of clusters. Therefore, it is important to choose an appropriate number of clusters.
5. The main advantage of the watershed method [57]–[60] is automatic detection of the number of clusters.
6. FPGA are semiconductor devices that can be useful for fast processing of medical imaging.

## 2. PROPOSED METHODS AND IMPLEMENTATIONS

The author's proposed systems consists of 6 modules (Fig. 2.1):

- 1) calculation of relaxation time;
- 2) visualization of knee-joint;
- 3) segmentation of tissues and fluids;
- 4) analysis of tissues and fluids;
- 5) textual analysis of patient's information;
- 6) FPGA optimization.

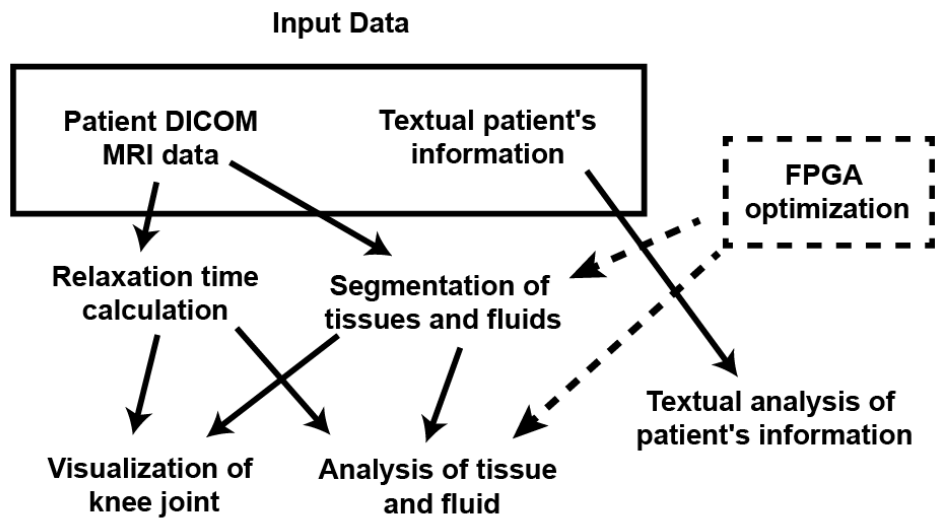


Fig. 2.1. Six modules.

### 2.1. Calculation of Relaxation Times

This work describes methods for calculation of relaxation times using one MRI image, two MRI images and multiple MRI images. The result of calculation (relaxation times) is shown by colourful images. Colourful image is useful for displaying changes of relaxation time. Image pixel colours (e.g., we can use Hue Saturation Value colour system) are displayed according to the calculated relaxation times.

Usually, a doctor gets the DICOM images from MRI. Pixels of each DICOM image contain intense value, which is proportional to MRI signal ( $S$ ). Let us assume that the MRI signal is approximately equal with DICOM image pixel containing intense value ( $SI$ ). This is shown in the following equation:  $SI \approx S$ . When we get MRI images, we know only the pixel values of MRI image ( $SI$ ) and images parameters  $T_E$  and  $T_R$ . But we want to know relaxation times  $T_2$  and  $T_1$ .

#### Relaxation time calculation by one MRI image

The method of “relaxation time calculation by one MRI image” is very useful for doctors because doctors usually use only one MRI image, which shows only one slice. This method is

very efficient because the time it takes to get an MRI image decreases. One MRI image is easier to obtain than multiple ones. If we use this method, we are able to save the MRI working time and reduce the RF (radio frequency) influence on patient's health.

But this method has some disadvantages, as it does not bear in mind some parameters, which influence pixels intense value ( $SI$ ). As a result, the calculation of relaxation time  $T_1$  and  $T_2$  is very approximate. This method is useful for displaying the changes of  $T_1$  and  $T_2$ .

For the calculation of times  $T_2$  and  $T_1$  it is assumed that proton density ( $\rho$ ) is constant and magnetic field power ( $B_0$ ) is constant. If assumed that the density ( $\rho$ ) is constant and magnetic field power ( $B_0$ ) is constant, then initial magnetization ( $M_0$ ) is constant.

$$S = M_0 \left[ 1 - \exp\left(\frac{-T_R}{T_1}\right) \right] \left[ \exp\left(\frac{-T_E}{T_2}\right) \right], \quad (2.1)$$

If we want to calculate relaxation time  $T_2$ , then we must use  $T_2$  weighted MRI image. When we use  $T_2$  weighted MRI image, we cannot consider the second part of Equation (2.1):  $(1 - \exp(-T_R / T_1))$ . So, now we have Equation (2.2):

$$T_2 = \frac{-T_E}{\ln\left(\frac{SI}{SI_{MAX}}\right)}, \quad (2.2)$$

where  $SI_{MAX} \approx M_0$ .

Now we can calculate  $T_2$ . For  $T_1$  calculation we can use the same method.

### Calculation of relaxation time by two MRI images

For the calculation of relaxation time, we can use two MRI images [61]. When we use two MRI images, we have more information and we can calculate relaxation time  $T_1 / T_2$  more precisely than in the previous method. For calculating  $T_1$  it is possible to use Equation (2.3):

$$T_1 = \frac{-T_{R1}}{\ln\left(\frac{SI_2 - SI_1}{SI_1}\right)}, \quad (2.3)$$

where  $T_{R1}$  is time to repeat the first image,  $SI_1$  is intense value of the first image,  $SI_2$  is intense value of the second image, and  $T_{R2} = 2T_{R1}$  and  $T_{E1} = T_{E2}$ . There is a proof (2.4) of Equation (2.3):  $T_{R1} / T_1$  are denoted by letter ( $a$ ).

$$\begin{aligned} \frac{SI_2 - SI_1}{SI_1} &= \frac{M_0 [1 - \exp(2a)] \cdot \exp\left(\frac{-T_E}{T_2}\right) - M_0 [1 - \exp(a)] \cdot \exp\left(\frac{-T_E}{T_2}\right)}{M_0 [1 - \exp(a)] \cdot \exp\left(\frac{-T_E}{T_2}\right)} = \\ &= \frac{[1 - \exp(2a)] - [1 - \exp(a)]}{1 - \exp(a)} = \frac{-\exp(a) \cdot \exp(a) + \exp(a)}{1 - \exp(a)} = \frac{\exp(a)[1 - \exp(a)]}{1 - \exp(a)} = \exp\left(\frac{-T_{R1}}{T_1}\right). \end{aligned} \quad (2.4)$$

### Calculation of relaxation time by multiple MRI images

For the calculation of relaxation time, we can use many MRI images [62]. This method provides the possibility to modulate the relaxation process. Usually when we use this method,

we have 7 or 8 images, which show one slice (Fig. 2.2). These images have different  $T_E$  parameters (when we want to calculate  $T_2$ ), and TR parameters (when we want to calculate  $T_1$ ). So, for each pixel of an MRI image we have 7 or 8 intense values, which show signal intense in different times. This gives us the possibility to approximate the relaxation process. We can make the approximation for two parameters: initial magnetization ( $M_0$ ) and relaxation time ( $T_2$ ). To solve the approximation task, we can use the least square method and partial derivatives.

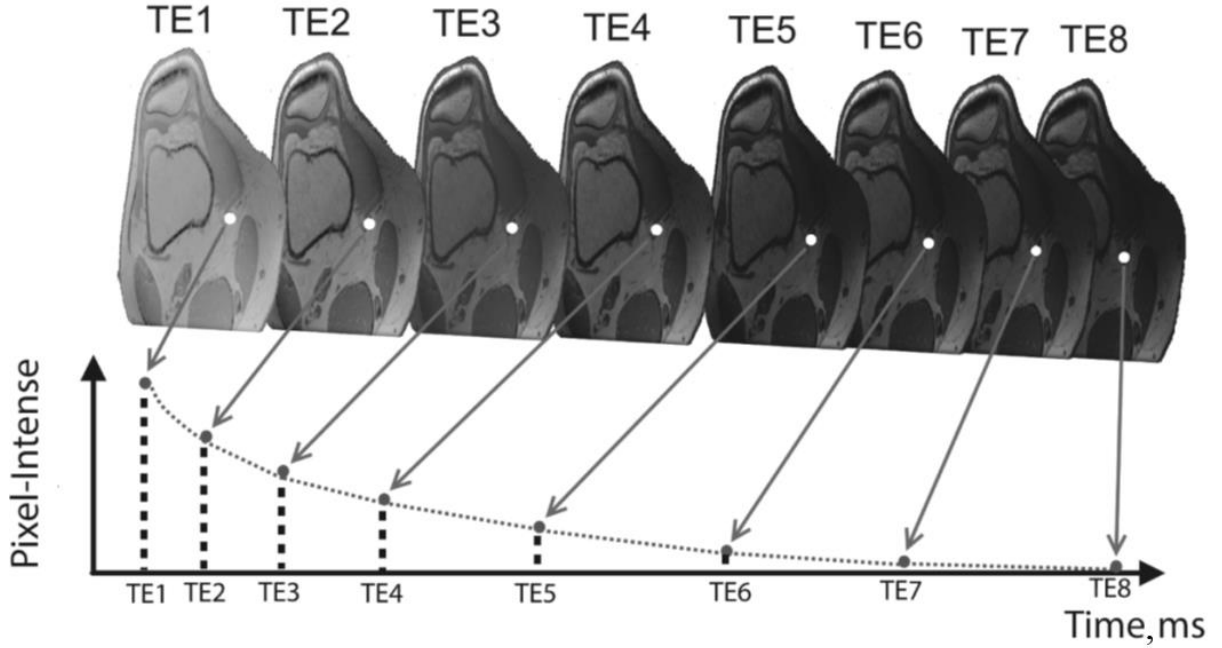


Fig. 2.2. Many MRI images, which reflect one slice (relaxation process  $T_2$ ).

We can see it from the following Formula (2.5):

$$\begin{aligned}
 S(M_0, T_2) &= \sum_{i=1}^n \left[ SI_i - M_0 \exp\left(\frac{-T_{Ei}}{T_2}\right) \right]^2 \rightarrow \min, \\
 \begin{cases} \frac{\partial S}{\partial M_0} = -2 \sum_{i=1}^n \left( e^{\frac{-T_{Ei}}{T_2}} (SI_i - M_0 e^{\frac{-T_{Ei}}{T_2}}) \right) = 0, \\ \frac{\partial S}{\partial T_2} = -\frac{2}{T_2^2} M_0 \sum_{i=1}^n \left[ e^{\frac{-T_{Ei}}{T_2}} (SI_i - M_0 e^{\frac{-T_{Ei}}{T_2}}) T_{Ei} \right] = 0, \end{cases} & (2.5)
 \end{aligned}$$

where  $M_0$  – initial magnetization;  $T_2$  – relaxation time;  $S$  – MRI signal;  $SI$  – intense value of image pixel;  $T_E$  – echo time;  $n$  – count of images.

## 2.2. Visualization of a Knee MRI Scanning Result

Usually, the result of MRI scanning is saved in the DICOM (Digital Imaging and Communications in Medicine) file. This file contains a knee image of signal intensities. This image of signal intensities is the main source of information for tissue analysis [63]. The range of signal intensity values is very wide: from 0 to 6000 (sometimes reaching 15 000).

However, this image has to be converted in order to display signal intensities on computer. The result of this conversion is a grayscale image. Grayscale image values are in the range from 0 to 255. Therefore, the grayscale image shows only a small part of the knee MRI scanning information. However, it is possible to show more information about knee tissues by using a colour image. The colour image values are in the range from 0 to 16 777 215. It is important to choose the most appropriate colour model, keeping in mind the human perception of colour [64]. One of the appropriate colour systems is hue-saturation-value (HSV) colour model. Special visualization methods of a knee MRI scanning result can be useful for displaying signal intensities.

Visualization of a knee MRI scanning result makes it possible to show more information about the knee tissues by using colour images. The task of visualization is to convert the intensity or relaxation time values into a colour image. Therefore, each value has an appropriate colour. For this purpose, it is possible to use Function (2.6). This function changes the parameter of a colour model (*CMP*). The change of a parameter depends on the values of intensities or relaxation times.

$$CMP = CR_{\text{MIN}} + VALUE \cdot STEP, \quad (2.6)$$

where *CMP* – modifiable parameter of colour model;  $CR_{\text{MIN}}$  – minimal *CMP* value; *VALUE* – value of intensity or relaxation time; *STEP* – the ration of *CMP* range to value range (2.7).

$$STEP = \frac{CR_{\text{MAX}} - CR_{\text{MIN}}}{VR_{\text{MAX}} - VR_{\text{MIN}}}, \quad (2.7)$$

where  $CR_{\text{MAX}}$  – maximal *CMP* value;  $VR_{\text{MAX}}$  – maximal visualization value;  $VR_{\text{MIN}}$  – minimal visualization value.

The colour image of the scanning result depends on the colour model. There are 2 colour models used in this work. The colour model allows to convert the MRI signal value to colour. BGRA model contains 4 components: blue, green, red, and alpha. It is not difficult to display the BGRA information on the RGB-screen. However, the HSV model is closer to the human perception of colour than the BGRA model. Therefore, HSV to RGB conversion is required for the visual display of HSV information. The HSV model contains 3 components: hue, value, saturation. There are 4 display modes in this work (Fig. 2.3).

1. BLUE RED: BGRA model – colour range is  $CR_{\text{MAX}} = 500$ ,  $CR_{\text{MIN}} = 0$ ; modifiable parameters (*CMP*) are blue and red components.
2. FULL HUE: HSV (hue, saturation value) model – colour range is  $CR_{\text{MAX}} = 360$ ,  $CR_{\text{MIN}} = 0$ ; modifiable parameters (*CMP*) is the hue component.
3. BLUE GREEN RED: HSV model – colour range is  $CR_{\text{MAX}} = 250$ ,  $CR_{\text{MIN}} = -10$ ; modifiable parameters (*CMP*) are hue.
4. GREEN RED: HSV model – colour range is  $CR_{\text{MAX}} = 150$ ,  $CR_{\text{MIN}} = -30$ ; *CMP* is hue.

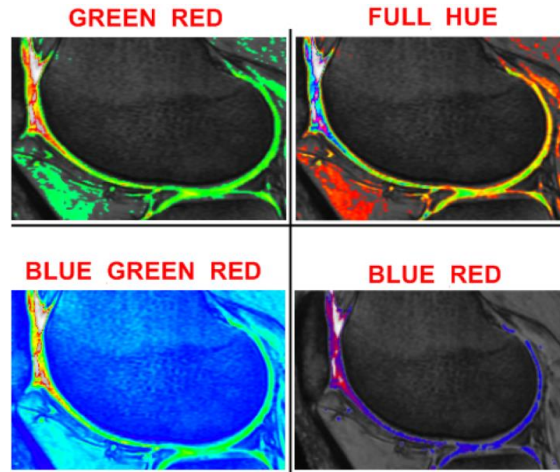


Fig. 2.3. Display modes of MRI scanning result.

The value range ( $VR_{MAX}-VR_{MIN}$ ) depends on the power of the MRI magnet. For example:

- 1) power of MRI magnet is 1.5 T – range of signal intensities is 0–6000;
- 2) power of MRI magnet is 3.0 T – range of signal intensities is 0–9000.

After relaxation time calculation, it is possible to get ranges of relaxation times:

- 1) range of relaxation time  $T_1$  is 0–6000 ms (3 T);
- 2) range of relaxation time  $T_2$  is 0–2000 ms.

Sometimes, it is necessary to show only one type of tissue (for example cartilage), in this case, it is possible to decrease the value range. This minimization, in turn, has made it possible to show more information about the proper tissue.

### 2.3. Tissue Dispersion Analysis

After automatic/semi-automatic tissue segmentation is finished, it is possible to perform knee analysis. The goal of this analysis is to detect the OA symptoms. There are many visual symptoms of OA: synovial effusion, eroded cartilage, narrowed joint space, subchondral bone lesion, osteophyte, inflamed synovium. However, these are symptoms of OA 2–4 grades. The first grade of OA is of most interest in respect to treatment benefits. The first grade is very important because at this stage it is possible to completely cure OA. However, there are no perceptible visual changes of a knee at this stage. Therefore, biochemical changes of a knee must be taken into account. There are some biochemical and physical changes of cartilage tissue at this stage: increase in the water content in cartilage; development of surface fibrillation; destruction of collagen fibers; increase in the  $T_{1\rho}$ ,  $T_2$  and proton density. These changes of cartilage tissue have an influence on the intensities of cartilage tissue. For this reason, it is possible to analyse intensities of cartilage tissue by calculating the dispersion (2.8) and histogram.

$$\begin{aligned}
D &= \overline{X^2} - (\overline{X})^2, \\
\overline{X} &= \frac{1}{n} \sum_{i=1}^n X_i, \\
\overline{X^2} &= \frac{1}{n} \sum_{i=1}^n X_i^2, \\
\sigma &= \sqrt{D},
\end{aligned}
\tag{2.8}$$

where  $D$  – dispersion of cartilage pixel intensities;  $\overline{X}$  – arithmetic mean of cartilage pixel intensities;  $\overline{X^2}$  – arithmetic mean of square cartilage pixel intensities;  $n$  – pixel count;  $\sigma$  – standard deviation.

## 2.4. Contour Searching in Medical Image

Contour searching process has 4 parts:

- 1) edge detection (Fig. 2.4);
- 2) tissue contour model creation (Fig. 2.5);
- 3) contour searching (Fig. 2.6);
- 4) improvement of contour searching result by using an active contour (Fig. 2.7).

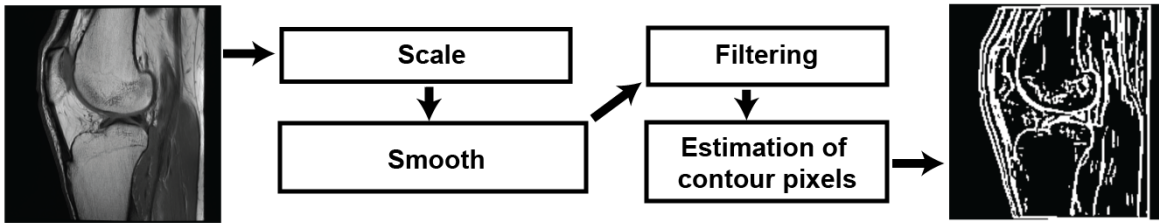


Fig. 2.4. Author's edge detection method.

The proposed edge detection method consists of four parts (Fig. 2.4):

- 1) scale (optional part) – allows to speed up preprocessing;
- 2) smooth (mean shift smooth [65] and Perona–Malika filter) – removes high frequency components, but does not remove borders of large segments;
- 3) filtering (edge detection) – filtering based on the second derivative;
- 4) estimation of contour pixels – allows removing unimportant pixels.

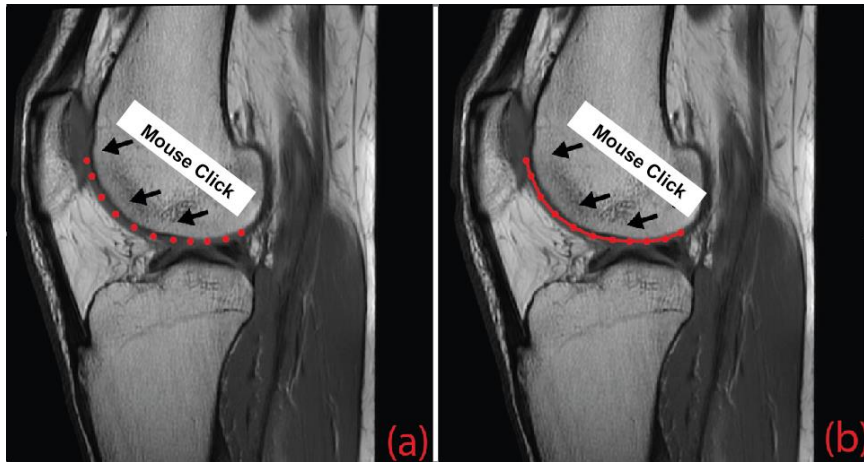


Fig. 2.5. Tissue contour model creation: a) point model; b) point-line model.

Tissue contour model creation has two modes (Fig. 2.5):

- 1) point model mode (fast matching) – creates point model that consists of points;
- 2) point-line model (slower matching) – consists of points and lines.

The model creation process is very simple. A doctor can create a model by a simple mouse click (Fig. 2.5).

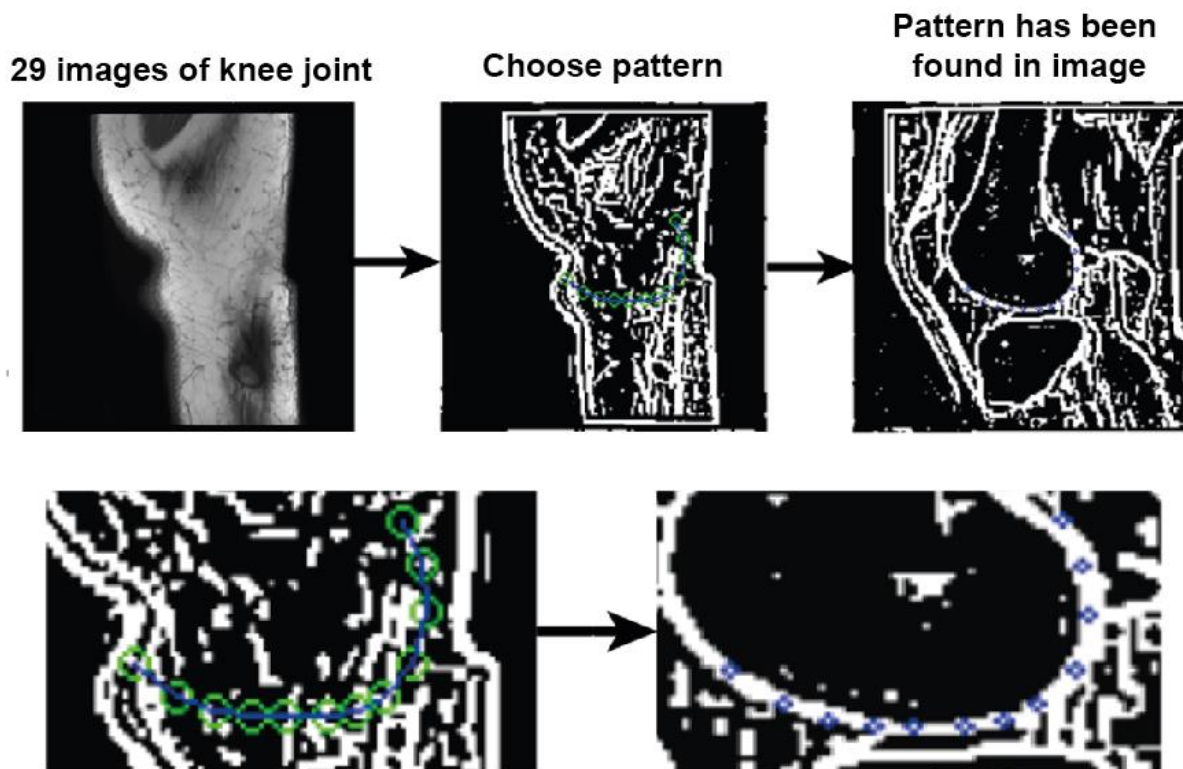


Fig. 2.6. Contour searching process.

Figure 2.6 shows the contour searching process. There are 3 steps (Fig 2.6):

- 1) selection of patient's MRI images (29 images of knee joint);
- 2) selection of contour model (pattern) – the doctor can select an appropriate contour model (cartilage, meniscus or bone model);
- 3) the developed software tries to find this contour model in the 3D space of MRI images.

The active contour model can improve contour searching results by using energy functional. Author's active contour implementation has 4 important parameters (Fig. 2.7):

- 1) stretch – internal energy coefficient;
- 2) curve – internal energy coefficient;
- 3) gradient – external energy coefficient;
- 4) radius – active contour degree of freedom.

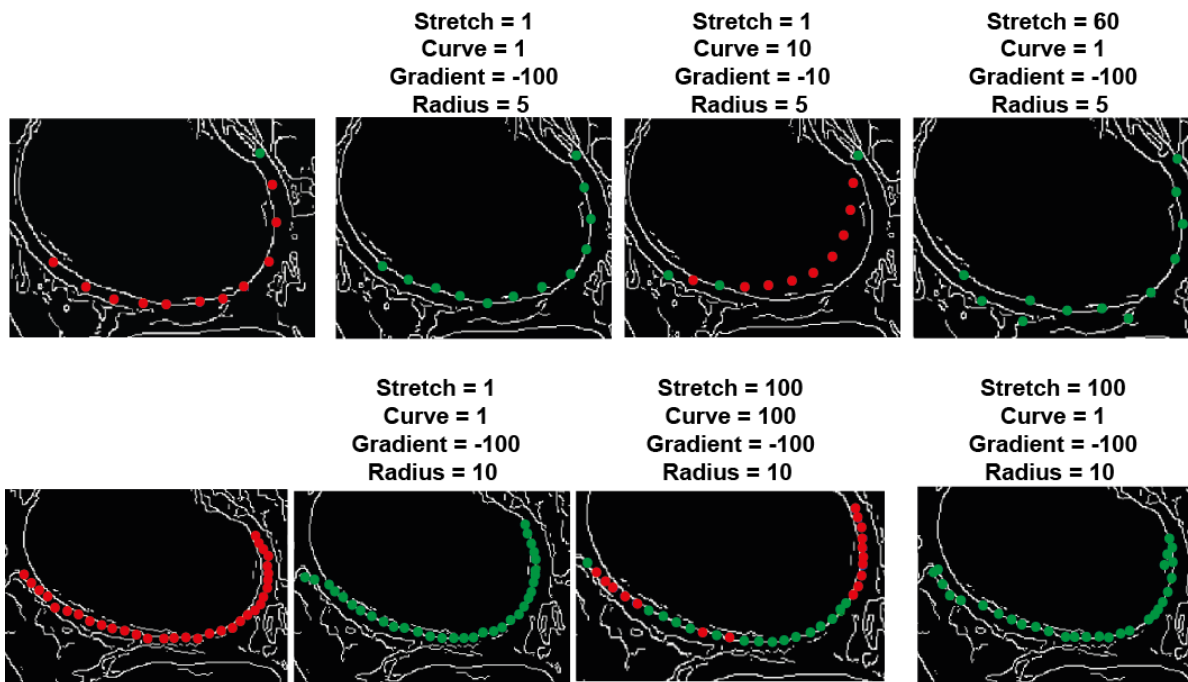


Fig. 2.7. The active contour model can improve edge detection results.

## 2.5. Automatic Detection of Increased Synovial Fluid Volume

Automatic detection of synovial fluid is a complicated task. The main problem is the geometric shape of synovial fluid. Synovial fluid does not have a fixed geometric shape. Therefore, it is impossible to use the contour model for this task. The author has tried different methods, and finds that the *k*-means and watershed are useful for this task.

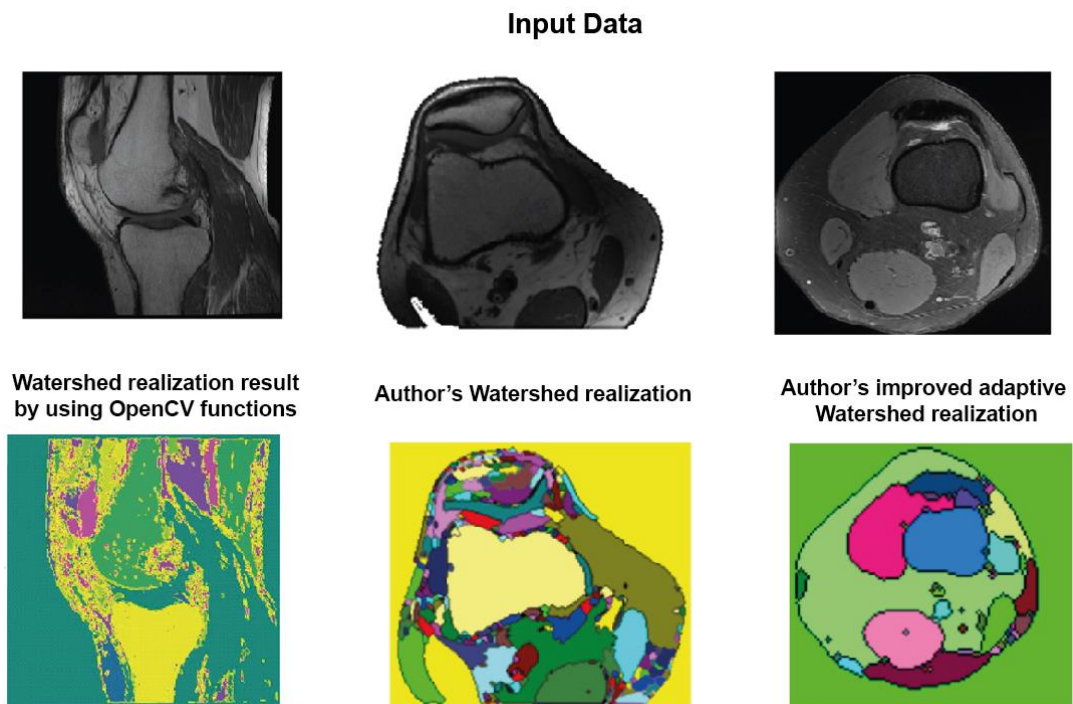


Fig. 2.8. Three of the author's watershed implementations.

The author has developed different modification of  $k$ -means and watershed (Fig. 2.8). Author's improved adaptive watershed implementation has the best results.

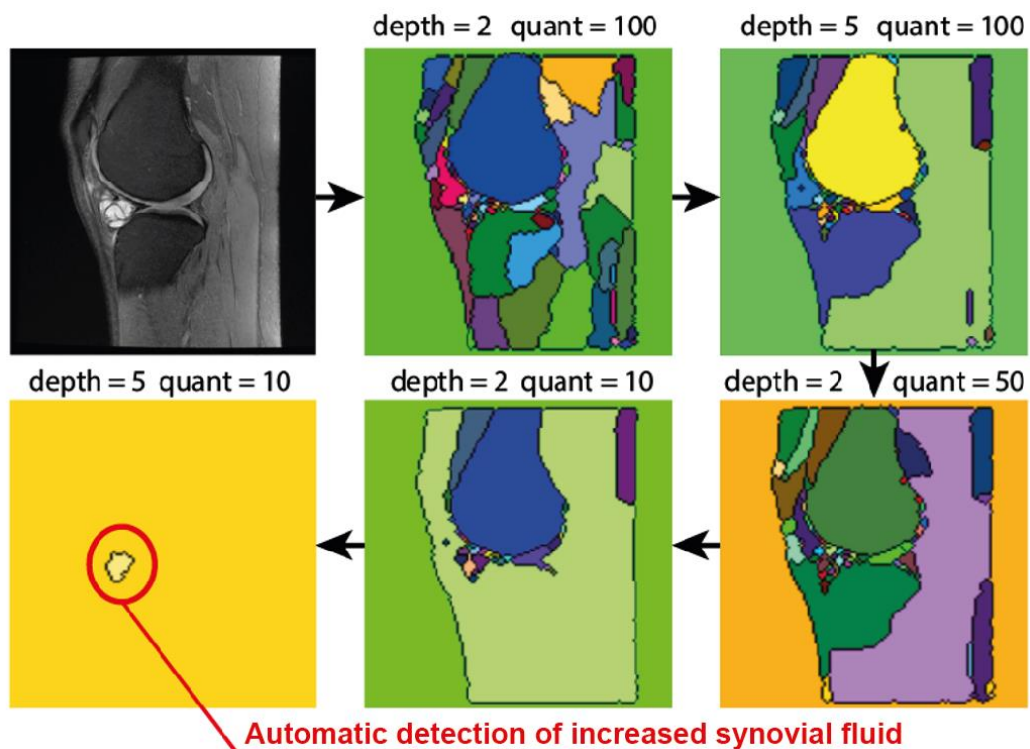


Fig. 2.9. Detection of increased synovial fluid by author's improved adaptive watershed.

It has two additional parameters: depth and quant (2.9).

$$S = F(\text{depth}, \text{quant}, I), \quad (2.9)$$

where  $S$  – segment set (or cluster set);  $I$  – MRI image (or image set in 3D space);  $\text{depth}$  – minimal depth of segment;  $\text{quant}$  – MRI image quantization coefficient;  $F$  – author’s improved adaptive watershed.

Figure 2.9 shows that the author’s improved adaptive watershed can get a lot of different segment sets ( $S$ ). The amount and shape of segment sets ( $S$ ) depends on two parameters – depth and quant (2.9). The improved adaptive watershed implementation has 8 modes. These modes have been described in approbation chapter. The experiments show that WAFSTTMS (WATERSHED\_ADAPT\_FAST\_TRESH\_TOP\_MAX\_SUM) is the best mode. Figure 2.10 shows the description of author’s improved adaptive watershed implementation (WAFSTTMS mode).

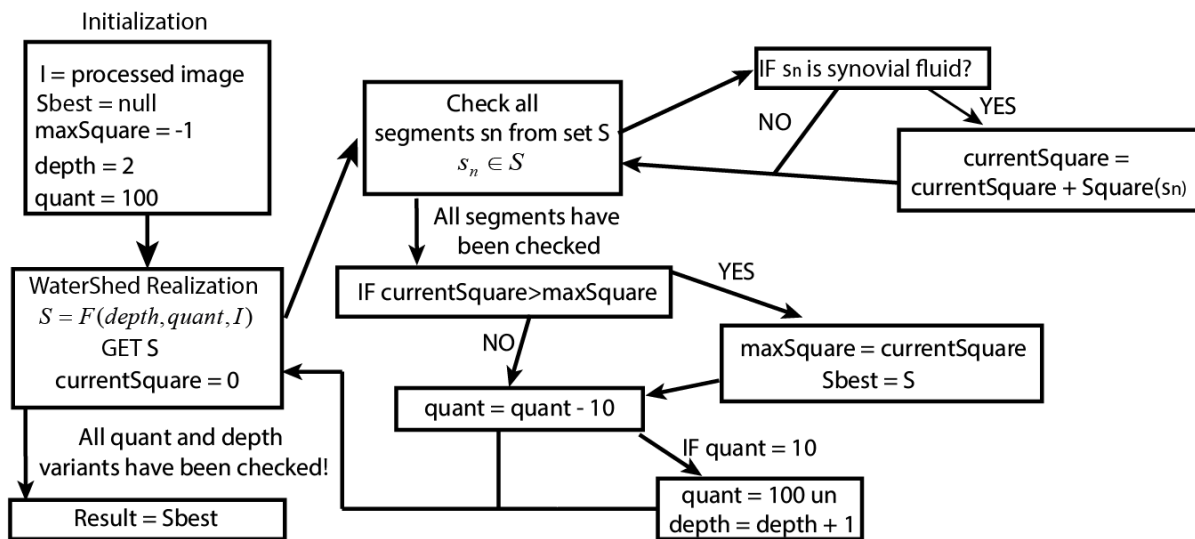


Fig. 2.10. Description of author’s improved adaptive Watershed implementation (WATERSHED\_ADAPT\_FAST\_TRESH\_TOP\_MAX\_SUM mode).

## 2.6. Textual Analysis of Patient’s Information

The author’s module for textual information analysis allows getting additional information about the state of patient’s knee-joint. This module provides a possibility to calculate osteoarthritis severity index and osteoarthritis probability index. These indexes can be calculated based on the patient’s responses.

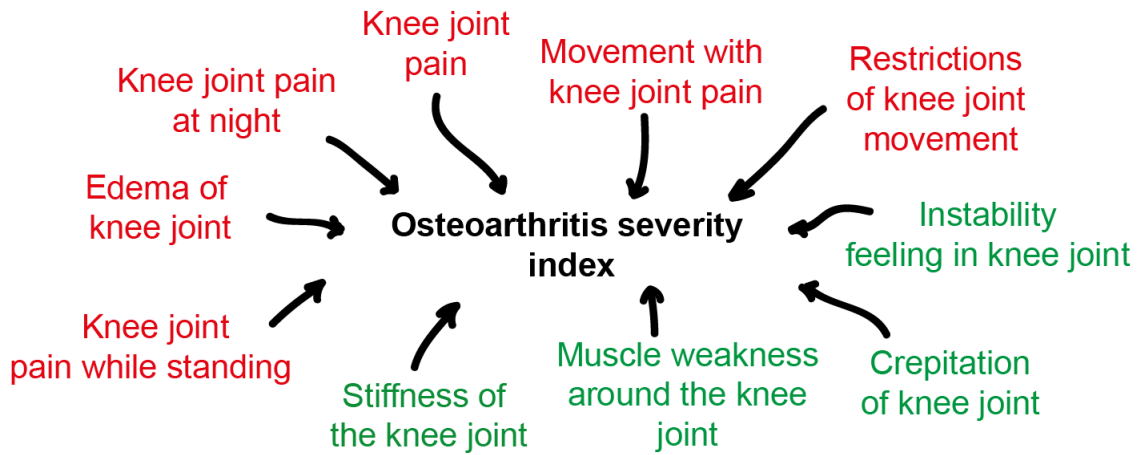


Fig. 2.11. Improved severity index of a knee-joint (red colour – important symptoms; green – less important symptoms).

Improved severity index is based on *BMI* (Quetelet index) and Lequesne index. Improved severity index depends on 22 patient’s answers. Figure 2.11 shows the main symptoms of OA that allow calculating the severity index.

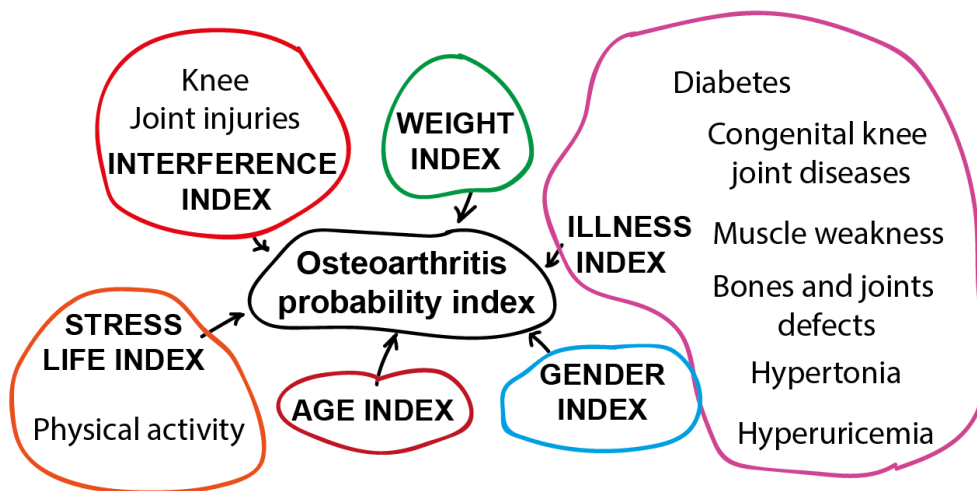


Fig. 2.12. Probability index of osteoarthritis.

Probability index of osteoarthritis depends on 6 of the author’s proposed indexes: WEIGHT INDEX, AGE INDEX, GENDER INDEX, STRESS LIFE INDEX, INTERFERENCE INDEX, and ILLNESS INDEX. These 6 indexes depend on 22 patient’s answers. These 6 indexes allow to create a patient model. For example, there are popular opposite OA patient models:

- 1) old overweight woman;
- 2) young sportsman with knee injuries.

The autor’s proposed method allows creating 2400 patient models by using the mentioned 6 indexes. In this work 27 OA patient models are shown by using the mentioned 6 indexes. These 27 models allow calculating the probability index of osteoarthritis.

## 2.7. FPGA Optimization

The author's program helps to reduce the execution time of the FPGA instruction that makes it possible to speed up the medical imaging processing [66], [67]. The author's program tries to remove unnecessary FPGA instruction elements. These elements are LUT (lookup table) components [68]. Figure 2.13. shows the comparison of FPGA minimization result. There are two programs:

- 1) SIS program (logic synthesis system) [69];
- 2) author's program.

The author's program results are better than SIS program results. The comparison of international results (Best LUT-6 Implementations – 2020)<sup>6</sup> shows that the author's program allows getting best minimization results in some FPGA instruction.

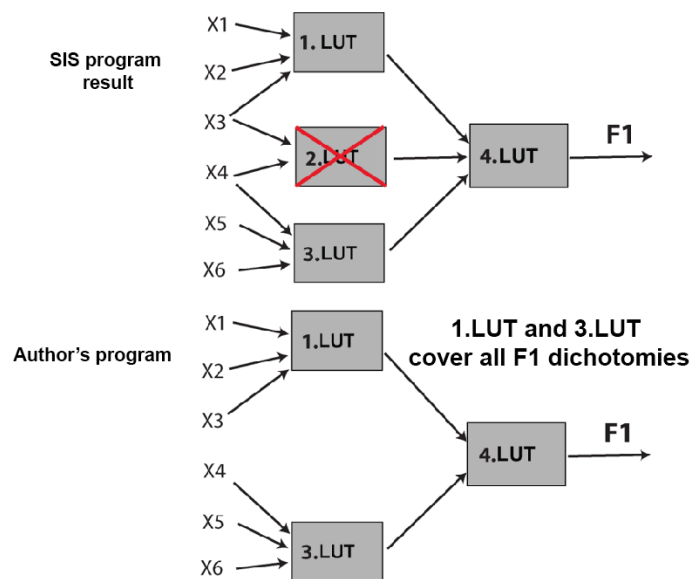


Fig. 2.13. Minimization of lookup table.

<sup>6</sup> Comparison of international results (Best LUT-6 Implementations – 2020) – [https://github.com/lsils/benchmarks/tree/master/best\\_results](https://github.com/lsils/benchmarks/tree/master/best_results).

### 3. APPROBATION

#### 3.1. Results of Visualization Methods

Experiments were performed with special visualization methods, aiming to look for cartilage degeneration by using the HSV and BGRA colour models. These matching experiments used 5 display modes: MRI original image (monochrome), blue red (BGRA model), full hue (HSV model), blue green red (HSV model), and green red (HSV model). The results of these experiments (Fig. 3.1.) show that the highest number of observable changes of cartilage have been in HSV and BGRA colour models. The full hue display mode has the best result because of the wide range of hue values. These experiments were performed using 19 different MRI images.

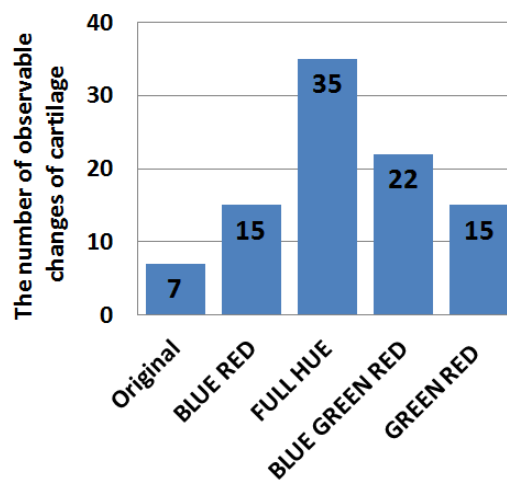


Fig. 3.1. Evaluation of visualization methods.

#### 3.2. Results of Histogram Analysis

The aim of this experiment is to compare the intensity dispersion of healthy and damaged cartilages. For these comparative experiments, proton density (PD) fat-suppressed (FS) MRI sequence was used. The MRI sequence  $T_E$  and  $T_R$  parameters have the following values:

- 1)  $T_E$  – from 26 ms to 29 ms;
- 2)  $T_R$  – from 2923 ms to 3170 ms.

The results of cartilage tissue analysis (Fig. 3.2) show that a healthy patient (green colour P2 and P5) has lesser standard deviation of cartilage signal intensity values than the patients with OA (red color P1, P3, P4, et al.).

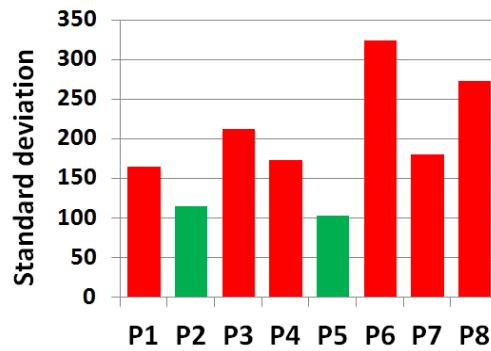


Fig. 3.2. Standard deviation of cartilage pixel intensities.

The aim of the second experiment is to compare healthy and damaged cartilages by using statistics parameters: mean, variance, homogeneity, skewness, kurtosis, entropy. For these comparative experiments, proton density (PD) 3D SAG CUBE HS VAL MRI sequence were used. The MRI sequence  $T_E$  and  $T_R$  parameters have the following values:

- 1)  $T_E$  – from 31 ms to 32 ms;
- 2)  $T_R$  – 1502 ms.

25 patients participated in this experiment. There were 10 healthy patients (H1...H10) and 15 patients (I1...I15) had problems with knee-joint (high OA probability). Each patient has 2 values (Fig. 3.3). The first value depends on lateral cartilage and the second value depends on medial value. Appendix 2 contains all statistics results. The results of cartilage tissue analysis (Appendix 2) show that a healthy patient (green colour) has lesser variance, kurtosis, and entropy and bigger homogeneity intensity values than the patients with knee-joint problems and possible OA.

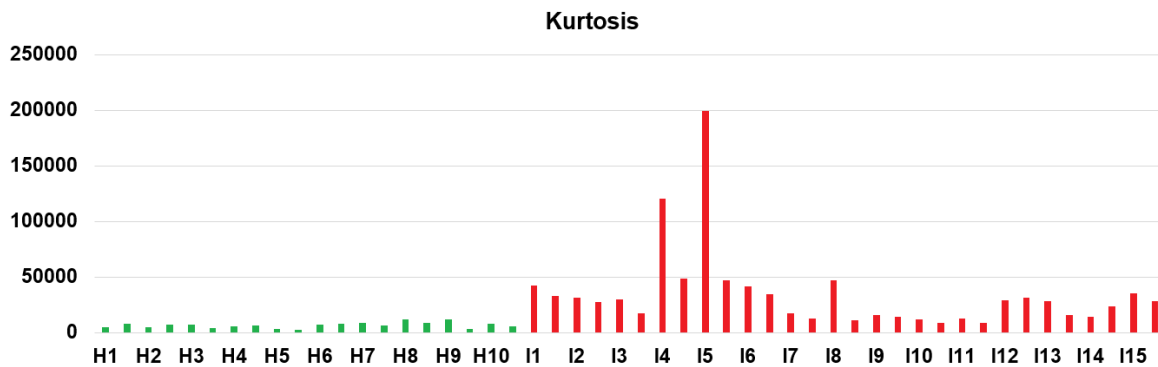


Fig. 3.3. Kurtosis of cartilage pixel intensities.

### 3.3. Modulating the Relaxation Process by Many MRI Images

Relaxation  $T_2$  process can be modulated by 8 MRI images that have different  $T_E$  (echo time). Therefore, these eight images contain information about proton energetic state at different moments in time. Thanks to this information, it is possible to approximate the relaxation process as shown in Fig. 3.4. This experiment has shown that various organic structures have a different relaxation process. In Fig. 3.4 we can see that muscle relaxation

process  $T_2$  is faster than the bone relaxation process. Different tissues have various relaxation times. Therefore, tissues classification problem can be solved by using the relaxation times.

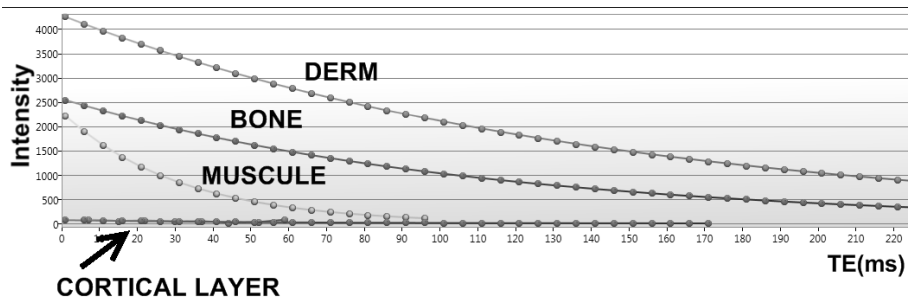


Fig. 3.4.  $T_2$  relaxation process.

### 3.4. Results of Image Pre-Processing and Segmentation

This experiment investigates the problem of pre-processing and segmentation. It is important to select the best possible combinations of methods to obtain the best results in reducing noise and artifacts [70]–[72]. The goal of this experiment is to compare 3 combinations of methods:

- only  $k$ -means clustering without image pre-processing;
- Perona–Malik filtering and  $k$ -means clustering;
- histogram equalization, Perona–Malik filtering and  $k$ -means clustering.

The experiment was evaluated by the following parameters:

- amount of images with high levels of noise and artifacts (HLNA);
- amount of images with low levels of noise and artifacts (LLNA);
- amount of images without noise and artifacts (NONA).

Each method used 273 processed images for processing.

Figure. 3.5 shows the estimation of the first combination ( $k$ -means clustering). There is a lot of noise and artifacts.

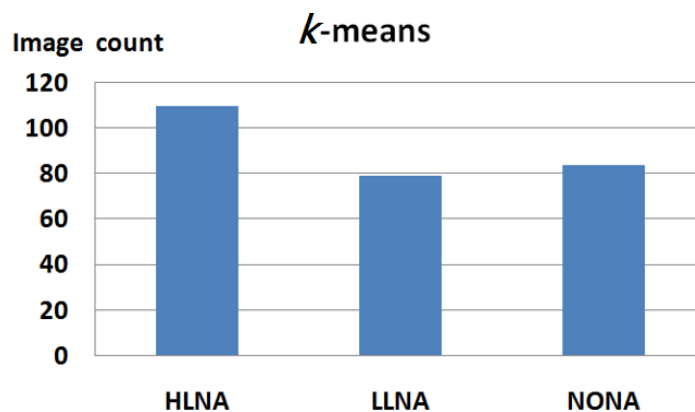


Fig. 3.5.  $k$ -means clustering estimation.

The results of the second combination (Perona–Malik filtering and  $k$ -means clustering) (Fig. 3.6) are much better than the  $k$ -means clustering. Figure 3.6 shows a reduction in noise and artifacts.

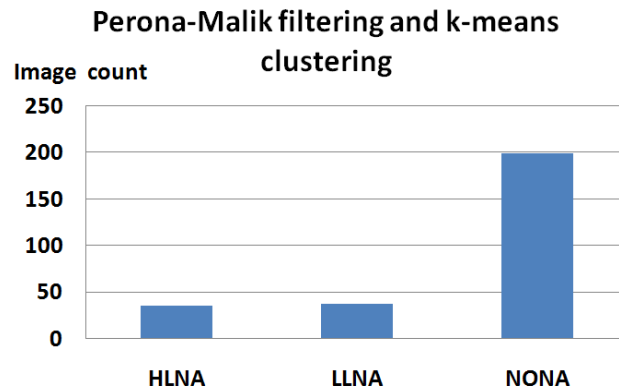


Fig. 3.6. Perona–Malik filtering and  $k$ -means clustering estimation.

The third combination (histogram equalization) had not led to any improvement in the results. Therefore, the second combination will be used further.

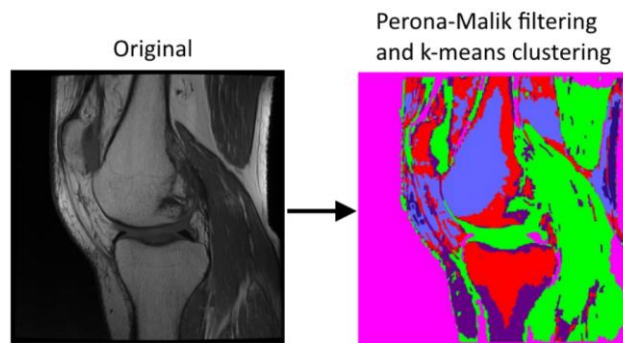


Fig. 3.7. The result of Perona–Malik filtering and  $k$ -means clustering.

The result of Perona–Malik filtering and  $k$ -means clustering can be seen in Fig. 3.7. There are different clusters (green, red and others). Green clusters contain voxels of cartilage and muscle. Blue and red clusters contain voxels of bone and fat. Magenta clusters contain voxels of background and meniscus. Therefore, it is impossible to recognize the tissue type using these clusters. It is for this reason that further experiments investigate the tissue recognition problem.

### 3.5. Knee-Joint Tissue Recognition

The easiest way to divide tissue voxels is to use the MRI signal intensities values.

#### MRI signal intensities

In this experiment DICOM images have the following parameters: sequence – FSE,  $T_R$  – 600 ms  $\pm$  100 ms,  $T_E$  – 10 ms  $\pm$  1 ms, and magnetic field power – 3 T. Table 3.1 shows the calculated mean and variance of tissue signal intensities. There are similar tissue types (in

Fig. 3.7 there is the same problem): bone and fat; cartilage and muscle; meniscus and background. Therefore, MRI signal intensities are very important for tissue recognition, but this tissue feature alone is not enough for precise tissue recognition. Therefore, it is helpful to use textural features.

Table 3.1

MRI Signal Intensities of Different Tissue Types

Tissues	Mean	Variance	Two sigma $\sigma$ range (95.4 %)	
			Min	Max
<i>(No tissue)</i> <i>Background</i>	106.40	10 291.47	1.00	309.29
<i>BONE</i>	3392.52	216 911.05	2461.05	4324.00
<i>FAT</i>	3957.12	461 584.90	2598.32	5315.92
<i>CARTILAGE</i>	1578.70	21 016.38	1288.76	1868.64
<i>MENISCUS</i>	661.65	16 162.14	407.39	915.91
<i>MUSCLE</i>	1418.56	36 280.27	1037.61	1799.51

### Analysis of textural features

In this experiment 64 textural features were calculated using GLCM (48 features) and GLSZM (16 features). These features were estimated for each tissue type. Therefore, it is possible to compare the features of tissue type.

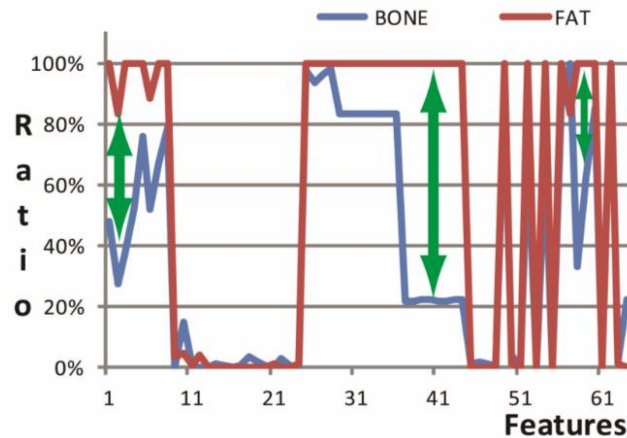


Fig. 3.8. Ratio between bone and fat.

The value of axis  $x$  is 64 features, and the value of axis  $y$  (3.1) is the ratio between the maximal feature value and an analysed tissue feature value.

$$ratio = \frac{f_{cur}(i)}{f_{max}(i)}, \quad (3.1)$$

where  $f_{cur}$  – currently analysed feature value;  $f_{max}$  – maximal feature value;  $i$  – feature number (from 1 to 64).

In the first part of the experiment the similar tissue features are compared by the mean value of the features. The results of the first part of the experiments for bone and fat tissue can be seen in Fig. 3.8.

In the second part of the experiment the similar tissues are compared in the value of the features. The point of this experiment is to find the essential similar tissue features. The results for cartilage and muscle features (number of experiments is 106) are shown in Table 3.2. There are 4 important features (uniformity, homogeneity, vertical correlation and diagonal correlation), the value of these features for muscle is greater than the value of these features for cartilage. And there is one important feature (dissimilarity), the value of this feature for cartilage is greater than the value of this feature for muscle. The rating for each feature is based on the confidence level.

Table 3.2

Feature Comparison Between Cartilage and Muscle

Number of features	Feature	Is greater for	Confidence
58 – GLZM	Uniformity	Muscle	0.821
15 – GLCM	Homogeneity	Muscle	0.755
14 – GLCM	Dissimilarity	Cartilage	0.745
24 and 48 – GLCM	Correlation (vertical and diagonal 135)	Muscle	0.745

The results for bone and fat, meniscus and background are shown in Table 3.3. It is possible to recognize the tissue type using the important features and the confidence levels.

Table 3.3

Feature Comparison Between Background and Meniscus, Bone and Fat

	Feature number/s	Feature	Is greater for	Confidence
Background and Meniscus	58 – GLZM	Uniformity	Background	0.990
	57 – GLZM	Spectral homogeneity	Background	0.990
	51 – GLZM	Low gray level zone emphasis	Meniscus	0.979
	55 – GLZM	Large zone low gray level emphasis	Meniscus	0.979
Bone and Fat	8 – GLCM	MEANX	Fat	0.843
	33 – GLCM	MEANY	Fat	0.843
	51 – GLZM	Low gray level zone emphasis	Bone	0.796

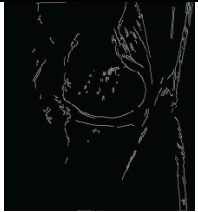
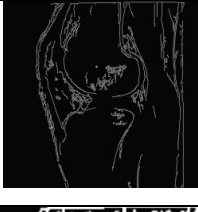
### 3.6. Results of Contour Searching in Medical Image

#### Results of edge detector

Table 3.4 shows the results of Canny [73] and author's approach. The results of Canny method consist of thin lines. The results of the author's approach consist of bold lines. These bold lines are useful for fast contour searching. If the region of interest is large, then contour searching can take a lot of time. Therefore, the results of the author's approach allow accelerating the contour searching process. Canny results can be useful for further contour improvement (contour alignment) by using active contour model.

Table 3.4

Comparison of Results of Edge Detectors (Full Variant – Appendix 1)

<b>Original</b>			
Canny	Threshold (upper and lower) 10/100		
	Threshold 100/200		
	Threshold 100/250		
<b>Proposed approach</b>			

## Results of contour searching

The aim of this experiment is to evaluate the proposed approach for contour searching. For these estimative experiments, relaxation time ( $T_1$ ) fat-suppressed (FS) MRI sequence were used. The MRI sequence  $T_E$  and  $T_R$  parameters have the following values:

- 1)  $T_E$  – from 8 ms to 11 ms;
- 2)  $T_R$  – from 661 ms to 814 ms.

20 patients have participated in this experiment. This experiment consists of 5 parts:

- 1) cartilage (of femur bone) contour searching by 13 points and 11 lines model of contour;
- 2) cartilage (of femur bone) contour searching by 15 points model of contour;
- 3) femur bone contour searching by 24 points and 23 lines model;
- 4) femur bone contour searching by 20 points model;
- 5) femur bone contour searching by 8 points and 7 lines model.

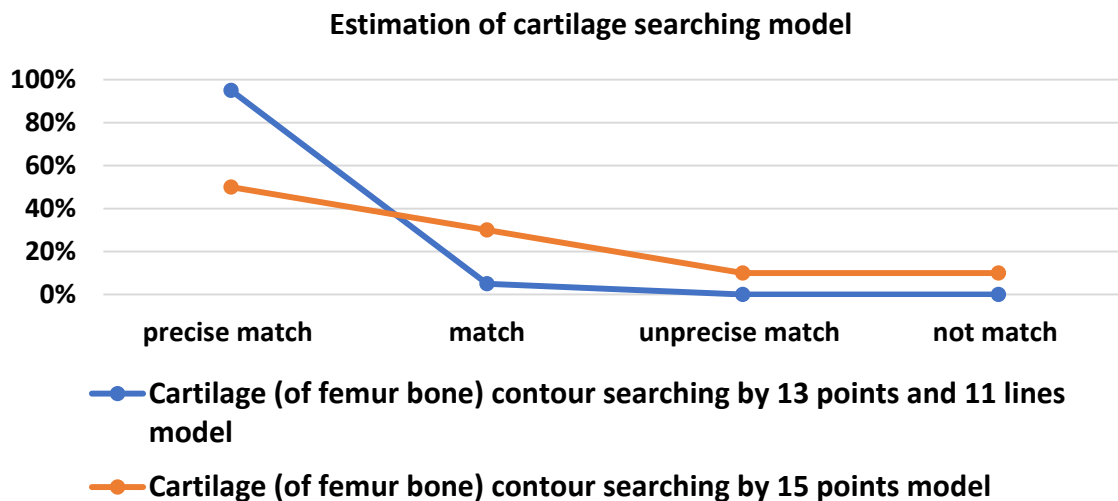


Fig. 3.9. Estimation of cartilage searching model.

The experiment was evaluated on the following scale:

- 1) precise match – match percentage is from 85 % to 100 %;
- 2) match – match percentage is from 70 % to 85 %;
- 3) unprecise match – match percentage is from 50 % to 70 %;
- 4) not match – model does not match.

Figure 3.9 shows the results of two cartilage models. The contour searching by 13 points and 11 lines model has the best result. This model (13 p. and 11 l.) has *precise match* in 19 out of 20 experiments and *match* in 1 out of 20 experiments. The results of contour searching depend on cartilage contour model.

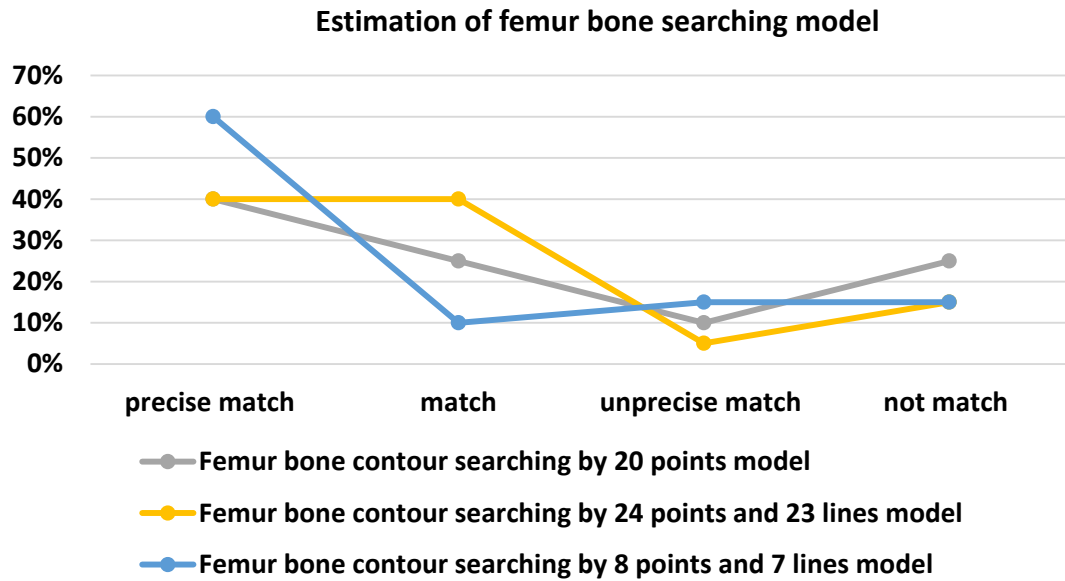


Fig. 3.10. Estimation of femur bone searching model.

Figure 3.10 shows the results of three femur bone models. The contour searching by 24 points and 23 lines model has the best result. This model (24 p. and 23 l.) has *precise match* in 8 out of 20 experiments, *match* in 8 out of 20 experiments, *unprecise match* in 1 out of 20 experiments and *not match* in 3 out of 20 experiments.

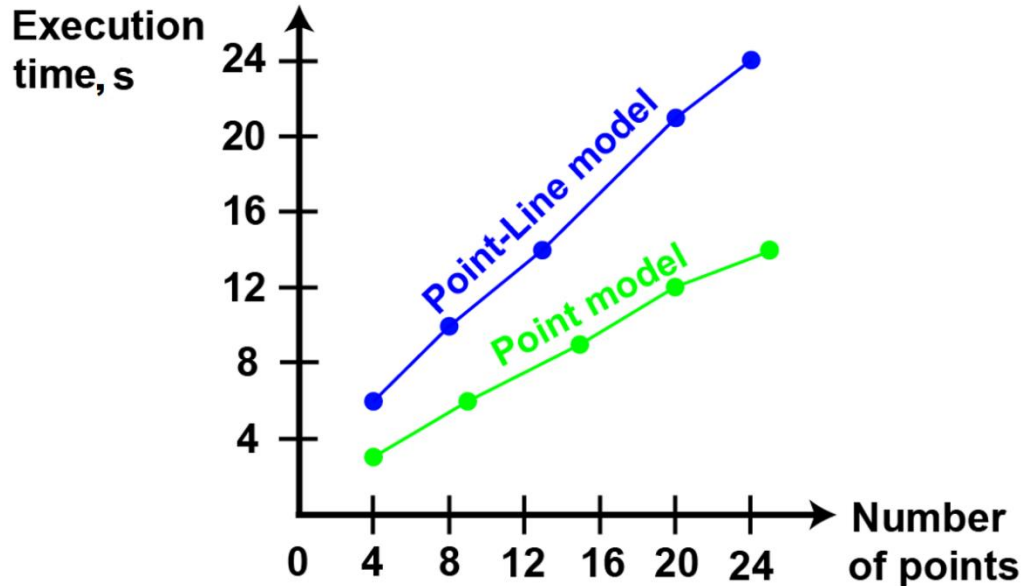


Fig. 3.11. Estimation of contour searching execution time.

Figure 3.11 shows the contour searching execution time. The point-line model works slower than the point model. The main advantage of the proposed contour searching method is execution speed. 1.8 million comparisons of modified tissue contour model with MRI images take an average of 12 seconds. This allows to check 1.8 million variants and choose the best variant from 1.8 million model modifications. These 1.8 million procedures of

checking and choosing take only an average of 12 seconds (in 6-year-old notebook PC). Contour searching makes it possible to automatically find the region of interest (bone, cartilage, meniscus ...).

Contour searching results (Figs. 3.9 and 3.10) have been obtained using one contour model (one cartilage contour searching model or one femur bone contour searching model). These contour searching results might have been improved by using a larger model set. It means that the contour searching task can be achieved by comparison of MRI images and many contour models. Then, of course, the comparison by one model takes less time than the comparison by many models.

### 3.7. Result of Automatic Detection of Increased Synovial Fluid Volume

The aim of this experiment is to compare methods for detection of increased synovial fluid. 12 patients have participated in this experiment. For these comparative experiments, proton density PD MRI sequences were used.  $T_E$  and  $T_R$  parameters of MRI sequences have the following values:

- 1) AXIAL PD,  $T_R = 2085\text{--}4205$  ms,  $T_E = 26\text{--}41$  ms, 3 T;
- 2) SAGITAL PD,  $T_R = 2500\text{--}3679$  ms,  $T_E = 31\text{--}38$  ms, 3 T.

The author has tried different methods for detection of increased synovial fluid and finds the  $k$ -mean and watershed are useful for this task. Figures 3.12–3.14 show the comparison of author's improved watershed implementations. There are eight segmentation modes:

- 1) WATERSHED\_SIMPLE\_TRESH\_2\_5 (WST\_2\_5) – watershed implementation with quant = 5 and depth = 2;
- 2) WATERSHED\_TRESH\_TOP\_2\_5 (WTT\_2\_5) – watershed implementation with topological analysis, quant = 5 and depth = 2;
- 3) WATERSHED\_ADAPT\_FAST\_TRESH\_TOP (WAFSTT) – adaptive watershed implementation with quant = from 5 to 25 and depth = from 2 to 3;
- 4) WATERSHED\_ADAPT\_FAST\_TRESH\_TOP\_MAX\_SUM (WAFSTTMS) – adaptive watershed that tries to increase the area of synovial fluid segments (quant from 5 to 25 and depth from 2 to 3);
- 5) WATERSHED\_ADAPT\_FAST\_SOFTTRESH\_TOP (WAFSTT) – adaptive watershed that has soft threshold (or greater range of synovial fluid features) for synovial fluid detection (quant from 5 to 25 and depth from 2 to 3);
- 6) WATERSHED\_ADAPT\_FAST\_SOFTTRESH\_TOP\_MAX\_SUM (WAFSTTMS) – WAFSTTMS with soft threshold (quant from 5 to 25 and depth from 2 to 3);
- 7) WATERSHED\_SIMPLE\_TRESH\_2\_10 (WST\_2\_10) – quant = 10 and depth = 2;
- 8) WATERSHED\_TRESH\_TOP\_2\_10 (WTT\_2\_10) quant = 10 and depth = 2.

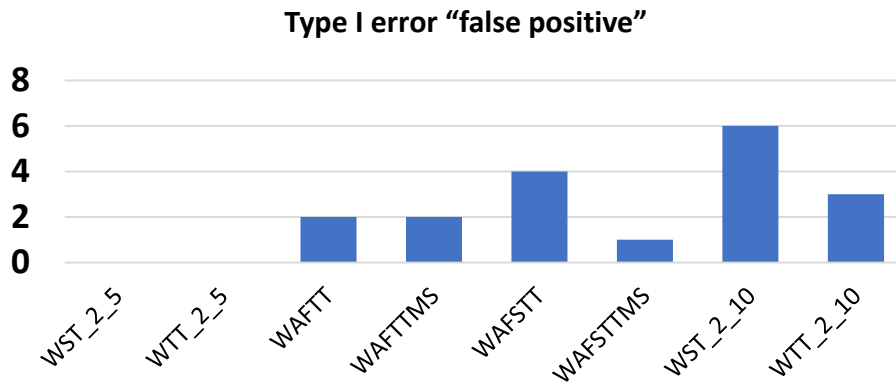


Fig. 3.12. Number of false detections of increased synovial fluid volume.

The descriptions of mode names:

- 1) TOP – topological analysis that checks synovial fluid segment location with respect to each other;
- 2) SOFTTRESH/TRESH – thresholds that are based on geometrical and textural synovial fluid features (Appendix 3).

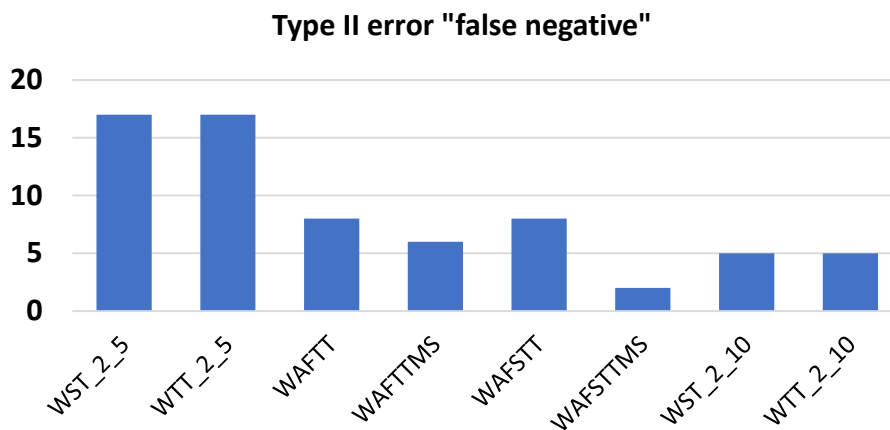


Fig. 3.13. Number of missed increases of synovial fluid volume.

Figure 3.12 shows that the WST\_2\_5, WTT\_2\_5 and WAFSTTMS modes have the smallest number of false detections. Figure 3.13 shows that the WST\_2\_10, WTT\_2\_10 and WAFSTTMS modes have the smallest number of missed increases of synovial fluid volume. Figure 3.14 shows that WAFSTTMS mode has the highest number of detections of increased synovial fluid volume.

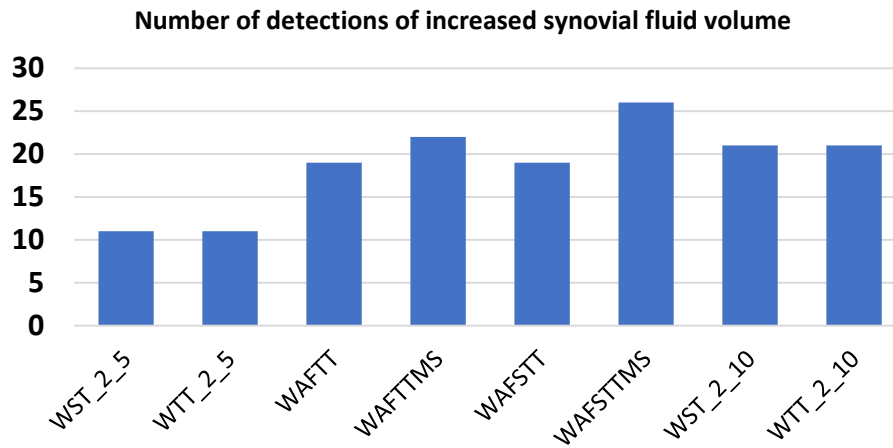


Fig. 3.14. Number of detections of increased synovial fluid volume.

The results of the experiment show that the synovial fluid has the following unique texture features: medium intensity value, barycentre, area highlighting (HGZE and LGZE [Appendix 3]). These texture features allow localizing synovial fluid and indicate an increase of synovial fluid. The author's program has 8 watershed modes of synovial fluid searching. The best synovial fluid searching mode is the WAFSTTMS mode.

## RESULTS AND CONCLUSIONS

As a result of the Doctoral Thesis, six new modules have been developed and are described in the practical part. These new modules have a lot of possibilities: calculation of relaxation times; human body fluid and tissue segmentation, calculation of features and defect detection; medical image pre-processing and visualization; optimization of medical image processing instruction; textual analysis of patient's information. These new modules allow solving the following tasks.

**Segmentation of tissues and fluids.** The medical image segmentation is a useful procedure for tissue and fluid analysis. The aim of medical image segmentation is the detection of pixels that contain tissues and fluids. When working with MRI images, there are a lot of segmentation problems: different image planes, many MRI parameters that strongly change the MRI signal, different sequences, artifacts, patient's movement and noise. Therefore, this work shows many solutions: cluster segmentation, region growing segmentation, interactive segmentation method, contour searching, and methods that are based on the watershed algorithm.

**Preprocessing of medical image.** The results of the first experiment show that the proposed combination of methods based on Perona–Malik filtering and  $k$ -means clustering are useful. The Perona–Malik filtering is very effective for reducing noise and artifacts. The  $k$ -means clustering is helpful for tissue segmentation. But  $k$ -means clustering alone is not enough for precise tissue recognition.

**Analysis of tissue textural features.** The results of the second experiment show that the MRI signal intensity feature alone is not enough for different tissue type detection. But the results of the third experiment show that it is possible to detect different type of tissues based on 65 features: MRI signal intensity, 48 features (GLCM) and 16 features (GLSZM). The results of this work could assist in the development of automatic knee-joint soft tissue recognition system that would save doctors' time. Experimental results can be useful for tissue analysis that allows starting treatment earlier, and therefore reducing the risk of tissue destruction.

**Automatic detection of increased synovial fluid volume.** The task of synovial fluid detection and localization is quite important. Synovial fluid increase (in the knee-joint) indicates that the patient has problems with the knee-joint [74]. The developed software makes it possible to find an object (tissue or fluid) of any shape. Synovial fluid can take any form. The results of the experiment show that the synovial fluid has unique texture features: medium intensity value, barycentre, area highlighting (HGZE and LGZE). These texture features allow localizing the synovial fluid and indicate increase of synovial fluid. The author's program has 8 watershed modes of synovial fluid searching. The best synovial fluid searching mode is the WAFSTTMS<sup>7</sup> mode. The author's program can automatically detect an increase of synovial fluid volume. Automatic detection of increased synovial fluid volume would save the doctor's time.

**Contour searching in medical image.** The developed software allows creating a model of tissue contour. Also, this software allows finding the selected 2D tissue contour in 3D

---

<sup>7</sup> WAFSTTMS – WATERSHED\_ADAPT\_FAST\_TRESH\_TOP\_MAX\_SUM mode.

space of MRI images. The results of the experiment show that the point-line model provides better accuracy than the point model. The main advantage of the proposed contour searching method is execution speed. 1.8 million comparisons of modified tissue contour model with MRI images take an average of 12 seconds. This allows to check 1.8 million variants and choose the best variant from 1.8 possible million model modifications. These 1.8 million procedures of checking and choosing take only an average of 12 seconds (in 6-year-old notebook PC). Contour searching makes it possible to automatically find the region of interest (bone, cartilage, meniscus ...).

**FPGA optimization.** The process of tissue identification, classification and localization can take quite a long time. Therefore, it is important to speed up this process. The author's program helps to reduce the execution time of the FPGA instruction that makes it possible to speed up the medical imaging processing.

**Relaxation time calculation.** In most situations, many MRI images (7 or 8 images) are used for relaxation time calculation [9], [75]. The proposed relaxation time calculation methods are universal, they allow calculating relaxation time by any MRI images count. It is very useful for the old MRI, which cannot get many MRI images in the same moment. "Relaxation time calculation by one MRI image" method is very effective because the time of MRI imaging is decreasing. We can get a single MRI image faster than many images. If we use this method, it will be possible to save the MRI working time and reduce the RF (radio frequency) influence on patient's health. When we use more MRI images, we have more information and we can calculate relaxation time  $T_1 / T_2$  more precisely. "Relaxation time calculation by many MRI images" method provides a possibility to modulate the relaxation process. All these methods allow calculating relaxation times  $T_2 / T_1$ . It is important to show the relaxation time changes by colourful images that allow displaying changes in relaxation times.

**Visualization of medical image.** Visualization of MRI scanning result makes it possible to show more information about tissues and fluids by using colour. The author's developed visualization module has two modes: mode 2D and mode 3D. The results of 2D visualization methods show that the use of HSV and BGRA model provide the most effective visualization of the cartilage degeneration. Moreover, the full hue display mode is the most sensitive to changes in cartilage intensity values. The experimental results show that thanks to the proposed methods a doctor can see cartilage pathogen zone and make an early OA diagnosis.

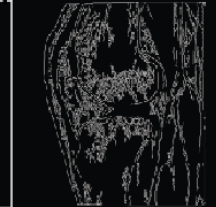
**Cartilage analysing.** The results of tissue analysis show that the intensity dispersion and intensity standard deviation of cartilage can help with the OA detection. The results of cartilage tissue analysis show that a healthy patient has a lesser standard deviation of cartilage signal intensity values than patients with OA.

**Textual analysis of patient's information.** The author's module for textual information analysis allows getting additional information about the state of patient's knee-joint. This module provides a possibility to calculate osteoarthritis severity index and osteoarthritis probability index. These indexes can be calculated based on the patient's responses.

Medical information technology expands the diagnostic possibilities of doctors. Also, this technology increases the quality and accessibility of medical services.

## **APPENDICES**

Comparison of Results of Edge Detectors

Original	Canny			Proposed Approach
	Threshold (upper and lower) 10/100	Threshold 100/200	Threshold 100/250	
				
				
				
				

Results of Cartilage Histogram Analysis

**Sequence:** 3D Sag PD Cube HS VAL;

**$T_R$ :** 1502 ms;  **$T_E$ :** 31–32 ms;

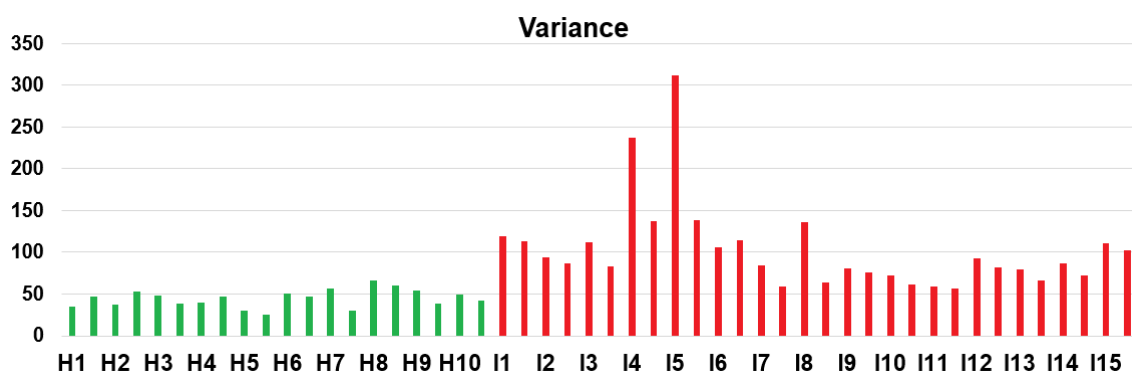
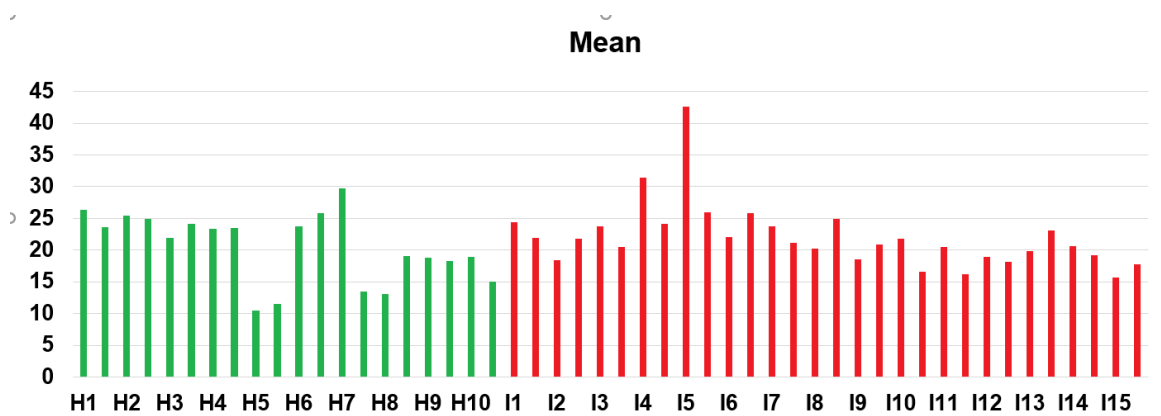
**Histogram quantization coefficient:** 7;

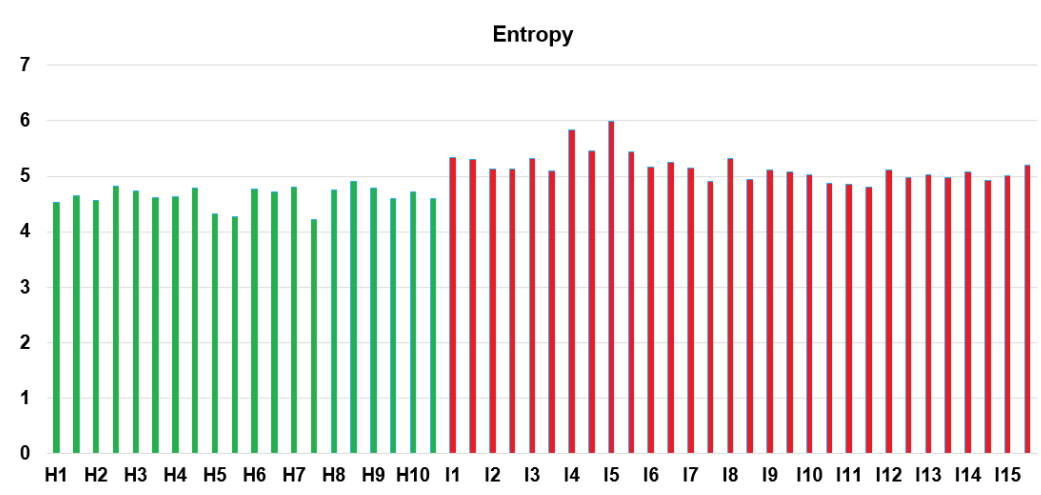
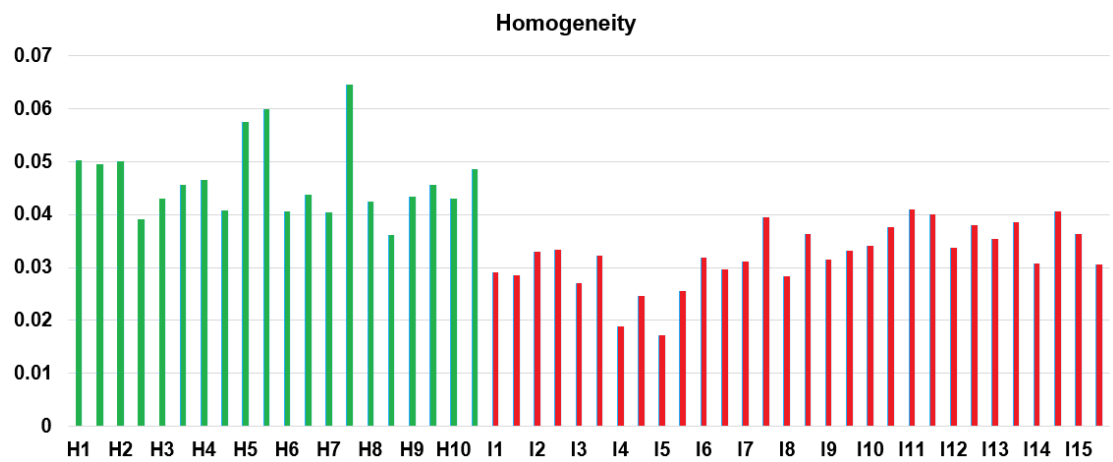
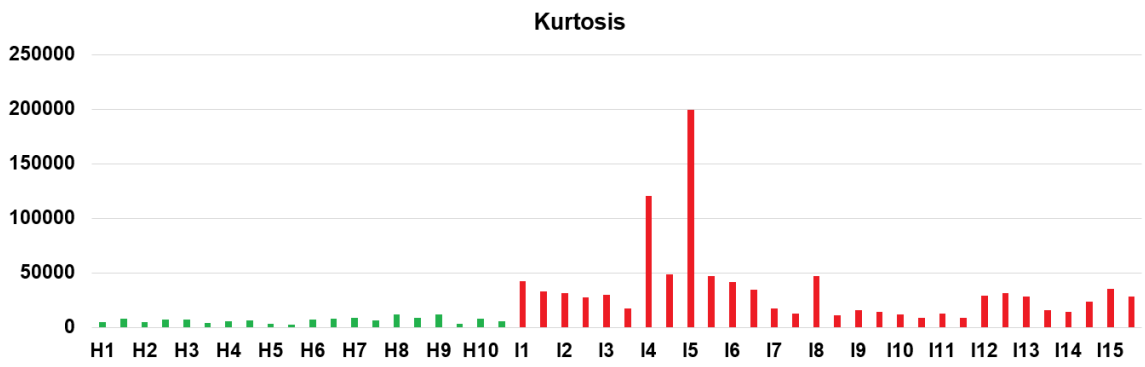
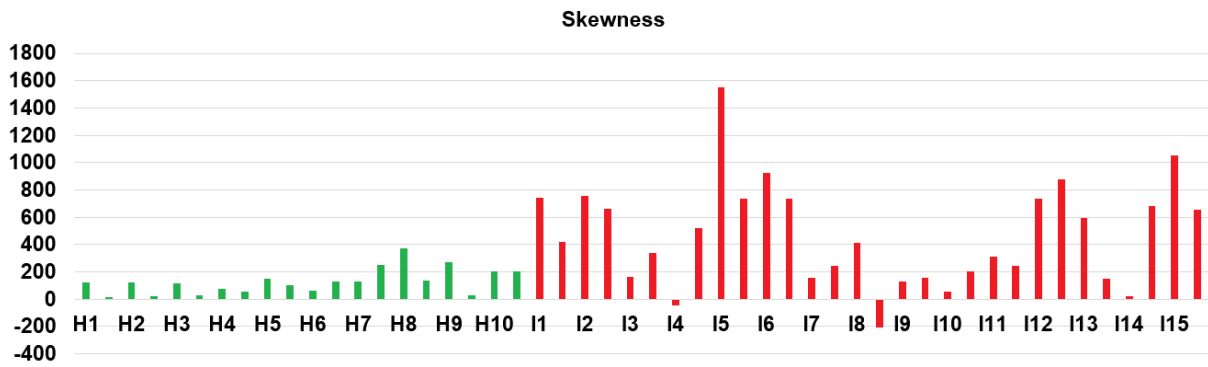
**Number of one segment pixels:** from 140 to 1136 pixels;

**Segment types:** lateral cartilage and medial cartilage;

**Data format:**

	Index Of Slice	Segment	Pixel count of segments	Mean	Variance	...
<b>H1</b>	34	lat. facets	870	26.40689655	34.88960761	...
<b>H1</b>	25	med. facets	318	23.63836478	47.5516099	...





## Feature Comparison Between Synovial Fluid and Other Tissues

<b>Feature number/s</b>	<b>Feature</b>	<b>Is greater for</b>	<b>Confidence</b>
GLCM (20, 21, 44, 45, 8, 9, 32, 33)	Mean $x$ and mean $y$	Synovial fluid	0.9999
GLZM (52 – HGZE)	High gray level zone emphasis	Synovial fluid	0.9999
GLZM (60 – BARYGL)	Barycenter on gray level	Synovial fluid	0.9999
GLZM (62 – VARGL)	Variance on gray level	Synovial fluid	0.9856
GLZM (56 – LZHGE)	Large zone high gray level emphasis	Synovial fluid	0.9784
GLZM (51 – LGZE)	Low gray level zone emphasis	Other tissues	0.9999
GLZM (53 – SZLGE)	Small zone low gray level emphasis	Other tissues	0.8561
GLZM (59 – ZPC)	Zone percentage	Other tissues	0.7985

## REFERENCES

- [1] Y. Zhang, J. M. Jordan, "Epidemiology of Osteoarthritis," *Clin Geriatr Med*, p. 355–369, 2010.
- [2] J. K. Timothy, "Astaxanthin for the Treatment of Osteoarthritis, a Large Unmet Medical Need," 2014.
- [3] L. Murphy, C. G. Helmick, "The impact of osteoarthritis in the United States. A population-health," 2010.
- [4] E.-W. Radue, M. Weigel, R. Wiest, H. Urbach, "Introduction to Magnetic Resonance Imaging for Neurologists," *ContinuumJournal*, pp. 1379–1398, 2016.
- [5] T. Kimple, T. Tuytschaever, "Increasing the Number of Gray Shades in Medical Display Systems – How Much is Enough?," *Journal of Digital Imaging*, p. 422–432, 2007.
- [6] I. N. BANKMAN, *Handbook of medical imaging processing and analysis*, Academic Press, 2008.
- [7] K. D. Toennies, *Guide to Medical Image Analysis Methods and Algorithms*, New York, 2012.
- [8] B. Evert, *Basic MRI Physics*, 2004.
- [9] J. P. Hornak, *The Basics of NMR*, 1997.
- [10] N. Gruszauskas, "Fast Spin Echo," 2006.
- [11] T. B. Smith, K. Nayak, "MRI artifacts and correction strategies," *Imaging Med.*, pp. 445–457, 2010.
- [12] A. Suponenkovs, Z. Markovics, A. Platkajis, "Computer Analysis of Knee by Magnetic Resonance Imaging Data," *ICTE*, vol. 104, pp. 354–361, 2016.
- [13] A. Suponenkovs, A. Platkajis, Z. Markovics, "Application of Magnetic Resonance Imaging and Computer Vision Technologies for Analysis of Knee Articular Cartilage Degeneration," *Lietuva Radiology Update*, 2018.
- [14] A. Suponenkovs, Z. Markovics and A. Platkajis, "Knee-joint tissue recognition in magnetic resonance imaging," *IEEE 30th Jubilee Neumann Colloquium*, 2018.
- [15] I. Supe, A. Suponenkovs, A. Platkājis, A. Kadiša, A. Lejnieks, "Detecting knee cartilage structural changes using magnetic resonance computed vision analysis in patients with osteoarthritis; preliminary results," *PROCEEDINGS OF LATVIAN ACADEMY OF SCIENCE*, 2020.
- [16] A. Suponenkovs, A. Glazs, A. Platkajis, "Development of methods for analysis of knee articular cartilage degeneration by magnetic resonance imaging data," *Journal of Physics: Conference Series*, vol. 818, no. 1, 2017.
- [17] A. Suponenkovs, M. Kovaļovsa, Z. Markovics, "Application of Computer Vision Technologies for Autonomous Pile Manipulation," *International Scientific and Practical Conference on Environment. Technology. Resources*, 2019.
- [18] A. Suponenkovs, J. Grabis, J. Kampars, A. Sisojevs, K. Pinka, G. Mosāns, R. Taranovs, A. Locmelis, "Application of Image Recognition and Machine Learning Technologies for Payment Data Processing Review and Challenges. 2017 5th IEEE Workshop on Advances in Information, Electronic and Electrical Engineering," *AIEEE*, 2017.
- [19] I. Lemberski, A. Suponenkovs, M. Uhanova, "LUT-oriented asynchronous logic design based on resubstitution," *DTIS*, 2019.

- [20] I. Lemberski and A. Suponenkovs, "Asynchronous logic design targeting LUTs," in *7th Mediterranean Conference on Embedded Computing*, 2018.
- [21] I. Lemberski, A. Suponenkovs, "Asynchronous logic one-level LUT design based on partial acknowledgement," *Microelectronics Journal*, pp. 53–61, 2018.
- [22] I. Lemberski, A. Suponenkovs, M. Uhanova, "LUT-Oriented Asynchronous Logic Design Based on Resubstitution," *DTIS*, 2019.
- [23] [Online]. Available: [https://github.com/lisils/benchmarks/tree/master/best\\_results](https://github.com/lisils/benchmarks/tree/master/best_results).
- [24] R. Varma, "Managing DICOM images: Tips and tricks for the radiologist," *The Indian journal of radiology and imaging*, 2012.
- [25] E. M. Haacke, R. W. Brown, M. R. Thompson, R. Venkatesan, "Magnetic Resonance Imaging Physical Principles and Sequence Design," p. 973, 1999.
- [26] C. Cooper, M. K. Javaid, N. Arden, "Epidemiology of osteoarthritis," *Atlas of Osteoarthritis*, pp. 21–36, 2015.
- [27] H. I. Roach, S. Tilley, "The Pathogenesis of Osteoarthritis," 2007.
- [28] A. Klusmann, H. Gebhardt, F. Liebers, V. E. Lars, "Individual and Occupational Risk Factors for Knee Osteoarthritis – Study Protocol of a Case Control Study," 2008.
- [29] I. U. Nasnikova, S. P. Morozov, P. A. Filisteev, "Magnetic resonance tomography: quantitative assessment methods in articular cartilage structure analysis of in patients with osteoartrosis," *Russian Electronic Journal of Radiology*, pp. 75–81, 2011.
- [30] M. Posadzy, J. Desimpel, F. M. Vanhoenacker, "Staging of Osteochondral Lesions of the Talus: MRI and Cone Beam CT," 2017.
- [31] E. Kuyinu, G. Narayanan, L. S. Nair, C. T. Laurencin, "Animal models of osteoarthritis: Classification, update, and measurement of outcomes," *Journal of Orthopaedic Surgery and Research*, 2016.
- [32] X. Wang, D. Hunter, J. Xu, C. Ding, "Metabolic triggered inflammation in osteoarthritis," 2014.
- [33] S. Krig, *Computer Vision Metrics: Survey, Taxonomy, and Analysis*, Apress , 2014.
- [34] J. Zunic, "Shape Descriptors for image analysis," *Mathematics Subject Classification*, 2010.
- [35] D. Chaudhuri, N. Kushwaha, I. Sharif, V. Gohri, "Unique Measure for Geometrical Shape Object Detection-based on Area Matching," *Defence Science Journal*, vol. 62, pp. 58–66, 2012.
- [36] J. Weickert, "Anisotropic Diffusion in Image Processing," 2008.
- [37] M. Wielgus, "Perona-Malik equation and its numerical properties," 2010.
- [38] K. Shrivastava, N. Gupta, N. Sharma, "Medical Image Segmentation using Modified K Means Clustering," *International Journal of Computer Applications*, vol. 103, 2014.
- [39] V. Grau, A. U. J. Mewes, M. Alcaniz, R. Kikinis, S. K. Warfield, "Improved Watershed Transform for Medical Image Segmentation Using Prior Information," *IEEE Transactions on medical imaging*, vol. 23, 2004.
- [40] L. Fu, B. Zhang, "A Co-Occurrence Matrix Algorithm Used for Medical Image," *International Conference on Computer Science and Network Technology*, 2011.
- [41] F. Albrechtsen, "Statistical Texture Measures Computed from Gray Level Cooccurrence Matrices," 2008.
- [42] R. Hamza, T. A. Al-assadi, "Genetic Algorithm to find optimal GLCM features," 2012.

- [43] K. S. H. R. Singh, "A comparison of gray-level run length matrix and gray-level co-occurrence matrix towards cereal grain classification," vol. 7, no. 6, 2016.
- [44] S. Mishra, B. Majhi, P. K. Sa, F. Siddiqui, "GLRLM based Feature Extraction for Acute Lymphoblastic Leukemia(ALL) Detection," *Springer*, 2018.
- [45] G. Thibault, J. Angulo, F. Meyer, "Advanced statistical matrices for texture characterization: application to dna chromatin and microtubule network classification," in *18th IEEE International Conference on Image Processing*, 2011.
- [46] J. A. Guillaume Thibault, "Efficient statistical/morphological cell texture characterization and classification," in *21th International Conference on Pattern Recognition (ICPR)*, Tsukuba, 2012.
- [47] A. Wimmer, G. Soza, J. Hornegger, "Shape-based Organ Segmentation," 2008.
- [48] K. R. Liu, "Pattern Recognition and Image Preprocessing," 2002.
- [49] V. Dutt, V. Chaudhry, I. Khan, "Pattern Recognition: an Overview," *American Journal of Intelligent Systems*, 2012.
- [50] G. L. Masala, "Pattern Recognition Techniques Applied to Biomedical Patterns," *International Journal of Health and Medical Engineering*, 2007.
- [51] M. Airouche, L. Bentabet, M. Zelmat, "Image Segmentation Using Active Contour Model and Level Set Method Applied to Detect Oil Spills," in *Proceedings of the World Congress on Engineering*, London, 2009.
- [52] M. Kass, A. Witkin, D. Terzopoulos, "Snakes: Active Contour Models," *International Journal of Computer Vision*, pp. 321–331, 1988.
- [53] D. Saraswathi, L. Sheela, "LUNG IMAGE SEGMENTATION USING K-MEANS CLUSTERING ALGORITHM WITH NOVEL DISTANCE METRIC," *IJRTER*, 2016.
- [54] A. Likas, N. Vlassis, J. J. Verbeek, "The global k-means clustering algorithm," *Elsevier Pattern Recognition*, pp. 451–461, 2003.
- [55] H.-H. Bock, "Origins and extensions of the k-means algorithm in cluster analysis," 2008.
- [56] C. Sundar, M. Chitradevi, G. Geetharamani, "An Analysis On The Performance Of K-Means Clustering Algorithm For Cardiotocogram Data Clustering," *IJCSA*, 2012.
- [57] F. Meyer, "The morphological approach to segmentation: the watershed transformation," 1993.
- [58] N. Salman, "Image Segmentation Based on Watershed and Edge Detection Techniques," 2006.
- [59] S. Ruparelia, "Implementation of Watershed Based Image Segmentation Algorithm in FPGA," 2012.
- [60] A. S. Kornilov, I. V. Safonov, "An Overview of Watershed Algorithm Implementations in Open Source Libraries," 2018.
- [61] L. Fanea, S. A. Sfrangeu, "Relaxation times mapping using magnetic resonance imagin," 2010.
- [62] C. P. Bruce, "Graphical Interface for Quantitative T1 and T2 Mapping of MRI Data," *Massachusetts Institute of Technology*, p. 119, 2001.
- [63] M. Mustra, K. Delac, M. Grgic, "Overview of the DICOM Standard," in *50th International Symposium ELMAR-2008*, Zadar, 2008.
- [64] W. M. A., "Human colour perception and its adaptation," *Computation in Neural Systems* 7, pp. 587–634, 1996.

- [65] D. Demirovic, "An Implementation of the Mean Shift Algorithm," *IPOL*, pp. 251–268, 2019.
- [66] D. P. Guragain, P. Ghimire, K. Budhathoki, "Implementation of FPGA Based Image Processing Algorithm Using Xilinx System Generator," *IRJET*, vol. 05, no. 01, p. 1457, 2018.
- [67] A. Gupta, H. Vaishnav, H. Garg, "Image Processing using Xilinx System Generator (XSG) in FPGA," *IJRSI*, vol. 2, no. 9, pp. 119–124, 2015.
- [68] U. Farooq, *Tree-Based Heterogeneous FPGA Architectures*, New York: Springer Science+Business Media, 2012.
- [69] E. Sentovich, L. Lavagno, H. Savoj, A. L. Sangiovanni-Vincentelli, "SIS: A System for Sequential Circuit Synthesis," 1998.
- [70] A. Stadler, W. Schima, A. Ba-Ssalamah, J. Kettenbach, E. Eisenhuber, *Artifacts in body MR imaging: their appearance and how to eliminate them*, Vienna, 2007, pp. 1242–1255.
- [71] K. Krupa, M. Bekiesinska-Figatowska, "Artifacts in Magnetic Resonance Imaging," *Pol J Radiol*, pp. 93–106, 2015.
- [72] A. Caliskan, U. Cevik, "3D Medical Image Processing by Using Filtering Methods," in *Science and Education Conference*, Diyarbakir, 2016.
- [73] T. A. I. T. Alang, T. T. Swee, M. A. As'ari, L. K. Meng, S. A. Malik, "Edge Detection in Magnetic Resonance Images using Global Canny Algorithm," in *International Medical Device and Technology Conference*, 2017.
- [74] K. K. Chan, R. W. Wu, "Symptoms, Signs and Quality of Life (QoL) in Osteoarthritis (OA)," in *Principles Of Osteoarthritis – Its Definition, Character, Derivation And Modality-Related Recognition*, Rijeka, InTech, 2012, pp. 25–41.
- [75] G. Blumenkrantz, S. Majumdar, "Quantitative magnetic resonance imaging of articular cartilage in osteoarthritis," *European Cell and Materials*, pp. 75–86, 2007.